THE UNIVERSITY OF MICHIGAN

INDUSTRY PROGRAM OF THE COLLEGE OF ENGINEERING

ELECTRON SPIN RESONANCE OF PARAMAGNETIC TUNGSTEN AND NIOBIUM SUBSTITUTION IN CALCIUM TUNGSTATE

Keh-chang Chu

A dissertation submitted in partial fulfillment
of the requirements for the degree of
Doctor of Philosophy in the
University of Michigan
Department of Nuclear Engineering
1967

December, 1967

IP-799

ensm

UMR1175

ACKNOWLEDGMENTS

The author wishes to express his sincere appreciation to Professor Kikuchi, Chairman of the doctoral committee, for his invaluable guidance and counsel throughout the course of this investigation. The author particularly wants to thank Dr. Lohr for the many hours spent in making suggestions and in evaluating progress. The helpful discussion and advice given by the other members of the committee are gratefully acknowledged. Many thanks are due to Dr. Mason, Mr. Morrison and Mr. Tseng for helpful discussions.

This work was carried out under research grants and contracts from NASA, Owens-Illinois, and Harry Diamond Laboratories. These supports are also gratefully acknowledged.

TABLE OF CONTENTS

LIST OF TABLES

LIST OF FIGURES

LIST OF FIGURES (Continued)

1. INTRODUCTION

The study of radiation effects in solids is a comparatively new branch of physical science which lies somewhere between nuclear physics and solid state physics. The goals of these studies are the identification of the defects, the understanding of how the defects are introduced and the understanding of the changes in the physical properties caused by these defects. Although studies of radiation effects have received their original motivation and continued support from the parent field of nuclear technology, the greatest cause of the development of this field is the value of the radiation effect as a means of studying the solid materials themselves. Radiation in many cases affords a very convenient means for introducing defects in a controlled manner into solids so that their effects on externally observable properties can be studied.

A powerful tool for the study of radiation effects in solids is electron spin resonance technique, when paramagnetic centers are created. The usefulness of this technique stems from the fact that the electron can be thought of as a microscopic electric and magnetic probe. Further probing can be made by applying uniaxial stress and studying the kinetics of the defects. Under favorable conditions, the structure of defect centers can be unequivocally identified from the electron spin resonance result and confirmed by the uniaxial stress probing. The concentrations of different kinds of defects can be measured separately and without difficulty. The measured values of defect concentrations then can be compared with the calculated values from radiation damage theories.

In this study we will show that reactor fast neutrons produce two prominent paramagnetic defects in $CaWO_4$ which are identified as due to paramagnetic tungstens associated with a nearest oxygen displacement and a nearest calcium displacement respectively. The measured concentration of oxygen vacancies is found to be in good agreement with the treatment of Kinchin and Pease.

Single crystals of calcium tungstate doped with rare-earth ions have been used extensively for solid state lasers.[1,2] This fact stimulated the optical as well as electron spin resonance studies of this crystal.[3-15] Although rare-earth ions can be introduced into calcium tungstate without a secondary compensating ion (creating a defect lattice), charge compensation by a second ion is generally preferred since it simplifies the fluorescent emission spectrum and electron spin resonance spectrum as well as to lower the threshold for laser action and to improve the mechanical properties of the crystal. The most common scheme, as outlined by Nassau,[16-18] is to compensate a Na^+ for each Ca^{++} ion replaced by a trivalent rare-earth ion. Although the structural match for these ions is nearly perfect, sodium presents problems because of its volatility at high melt temperature and its relatively low distribution coefficient. Compared with sodium compounds, niobates are considerably more stable and its distribution is much more favorable, being close to unity.

The electron spin resonance results of the rare-earth ions in calcium tungstate in general consist of both tetragonal and rhombic spectra[7-11] and the addition of charge compensators has the effect of reducing the intensity of the rhombic spectrum. There have been uncertainties about the sites of paramagnetic centers and the mechanism of charge compensation. An electron spin resonance study of niobium in

calcium tungstate will undoubtedly provide important information about the above mentioned problems. It will be shown that experimental results give direct evidence that niobium is one hundred percent substitutionally in tungstate site. Previously this was only inferred from chemical evidence. The niobium spectrum has the interesting property of splitting at low temperature and the temperature dependence of the spectrum clearly shows vibronic effects. Besides, the ESR of niobium has only been reported in a few cases, mostly in solution and in glass. Thus the study of niobium itself is of importance since it provides information of the comparatively little studied $4d^1$ electron configuration.

This research has been undertaken as part of a general program for studying radiation effects in laser materials at the Radiation Solid State Physics Laboratory of the Department of Nuclear Engineering, University of Michigan.

1.1 Physical Properties and Crystal Structure of $CaWO_4$.

There are several favorable features for a study of the system. Single crystals of calcium tungstate have been made commercially for use in gamma scintillation counters and as laser materials. This was made possible by a method of growing calcium tungstate single crystals using Czochralski technique due to Nassau and Broyer.[16]

The natural abundance and nuclear spin of tungsten isotopes are well known. The tungsten ESR signature consists of one central and two satellite lines with an intensity ratio of twelve to one as shown in Figure 1. The fact that tungsten ESR can be observed makes it feasible to obtain definite information about the irradiation produced paramagnetic centers.

Tungsten Paramagnetic Resonance Signature

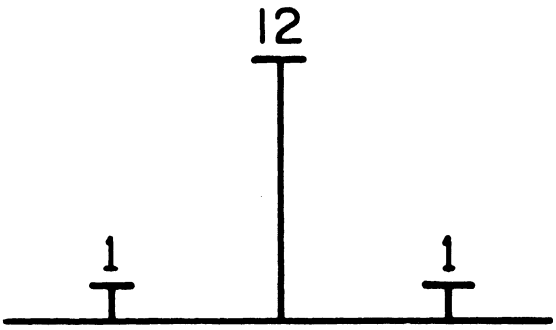

EVEN		ODD	
W^{180}	.122%	W^{183}	14.24%
W^{182}	25.80%	Z = 74	N = 109
W^{184}	30.68%	I = 1/2	
W^{186}	29.17%	$\mu = 0.115\mu_n$	
Total	85.77%		

Figure 1. Tungsten ESR Signature.

The crystal structure is well-known. This makes the identification of the irradiation produced paramagnetic centers possible. Recently, X-ray diffraction refinements of calcium tungstate crystal structure has been reported by Zalkin and Templeton[19] and neutron diffraction refinements reported by Kay, Fraser and Almodovar.[20] The results obtained by the two different methods are in excellent agreement These provide precise information of oxygen positions which were not available before.

Crystal Structure: Calcium tungstate is tetragonal with four molecules in the unit cell as shown in Figure 2. In the calculation of angles and distances the following diffraction data has been used.

Unit cell dimensions

$$a = b = 5.243 \text{ Å}$$

$$c = 11.376 \text{ Å}$$

The atoms are located as follows.

			(0, 0, 0;	1/2, 1/2, 1/2)
4	Ca	at	0, 0, 1/2;	0, 1/2, 3/4
4	W	at	0, 0, 0;	0, 1/2, 1/4
16	O	at	(x,y),z;	(y,x),z
			(x, 1/2-y),	1/4-z
			(y, 1/2-x),	1/4-z

Oxygen coordinates using a W atom as the origin are as follows.

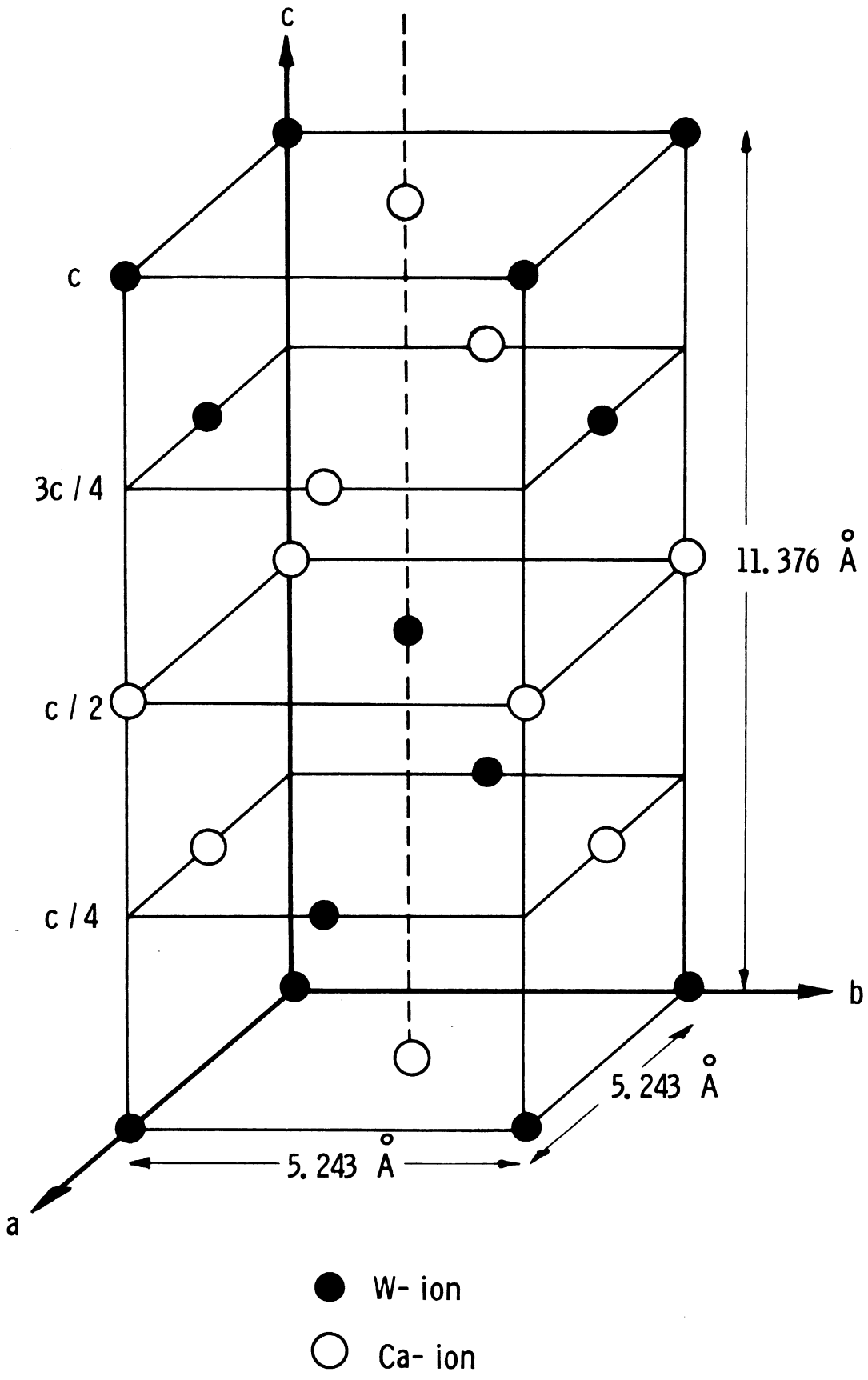

Figure 2. Metal Ions in $CaWO_4$ Unit Cell.

$$x = (0.2415 \pm 0.0014)\ a$$

$$y = (0.1504 \pm 0.0013)\ a$$

$$z = (0.0816 \pm 0.0006)\ c\ .$$

The structure of calcium tungstate crystal may be viewed as composed of tungstate WO_4^{--} anions ionically bonded to calcium Ca^{++} cations. The metallic sites are found on planes separated by a distance of $c/4$ from each other and perpendicular to the c-axis as shown in Figure 2. The local site symmetry of both calcium and tungsten is S_4 . Each tungsten is bonded to four nearest oxygens to form a slightly squashed tetrahedron with the W-O bond distance of 1.783 Å . The O-W-O angles are 113°27' (twice) and 107°56' (four times). The WO_4^{--} bisphenoid (tetrahedron distorted along one of the two-fold axes) and its projection on the (a,b) plane are shown in Figure 3.

On the other hand the nearest neighbors of the calcium atom are the eight oxygens at the vertices of two different bisphenoids as shown in Figure 4. The Ca-O distance are 2.44 Å and 2.48 Å respectively. The mirror-rotation axes S_4 of all these three bisphenoids coincide with the c-axis of the crystal.

1.2 Electron Spin Resonance

Since the pioneering investigation by F. Zavoisky[21] and by R. L. Cummerow and D. Halliday,[22] the phenomenon of electron spin resonance has been applied to a wide range of fields varying from the measurements of nuclear spins and magnetic moments to the study of biological systems such as oxidative enzymes,[23] ribonucleic acid (RNA) and deoxyribonucleic acid (DNA).[24] The electron spin resonance technique has also been successfully applied to a variety of problems in

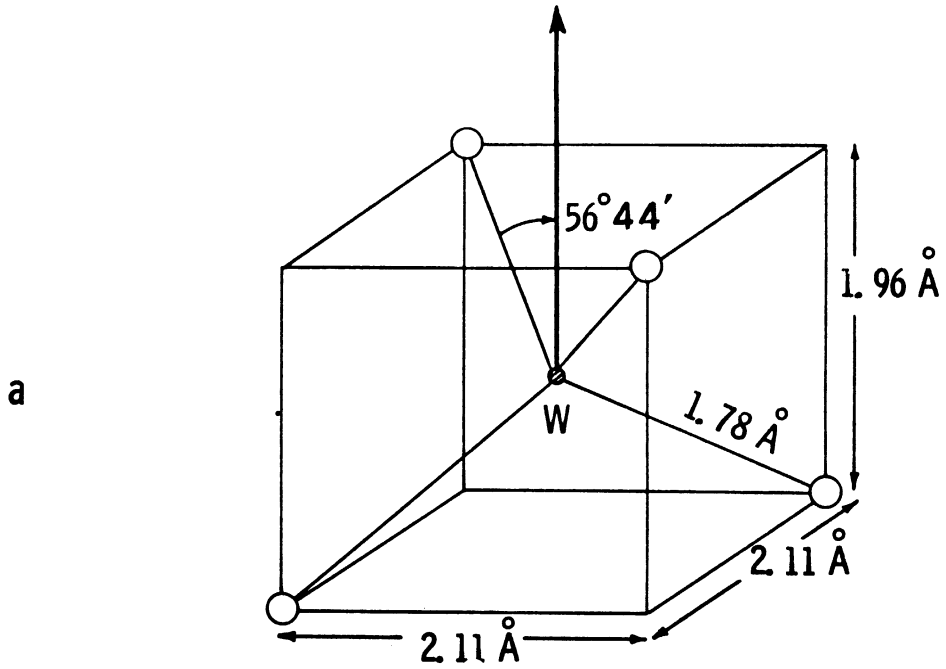

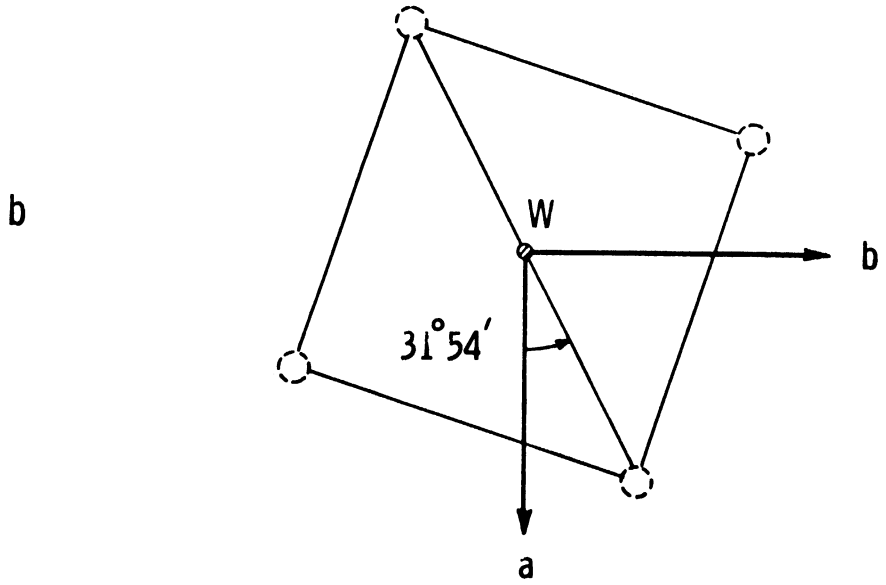

Figure 3. Projection of $(WO_4)^{--}$ Bisphenoid on the (ab)-plane.

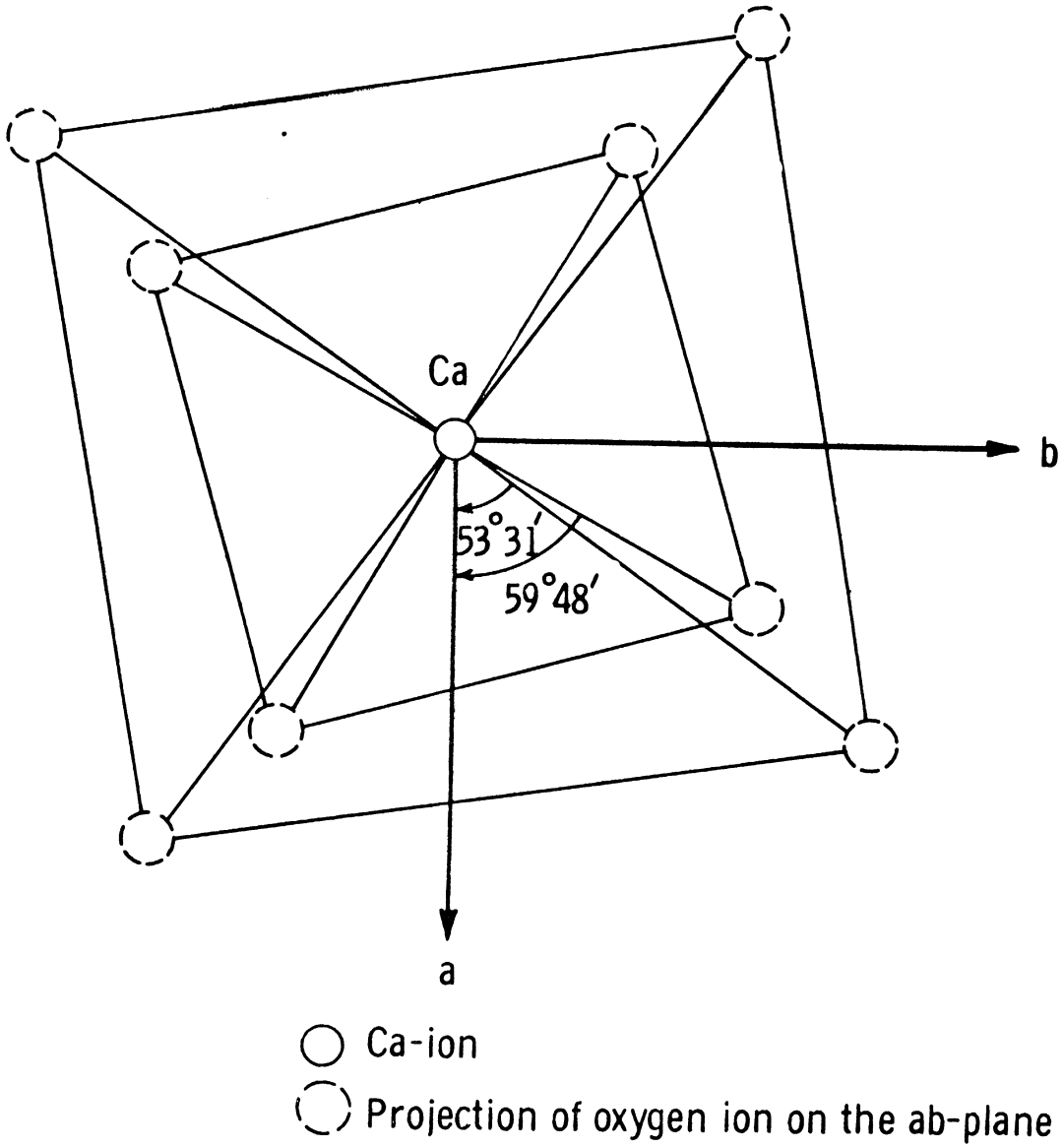

Figure 4(a). Projection of (Ca,O) Double-bisphenoid on the (ab)-plane.

a

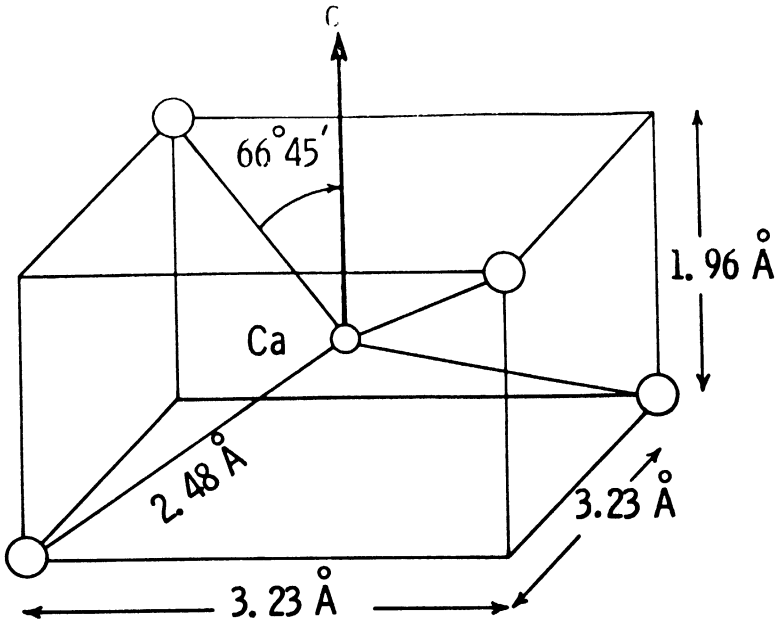

b

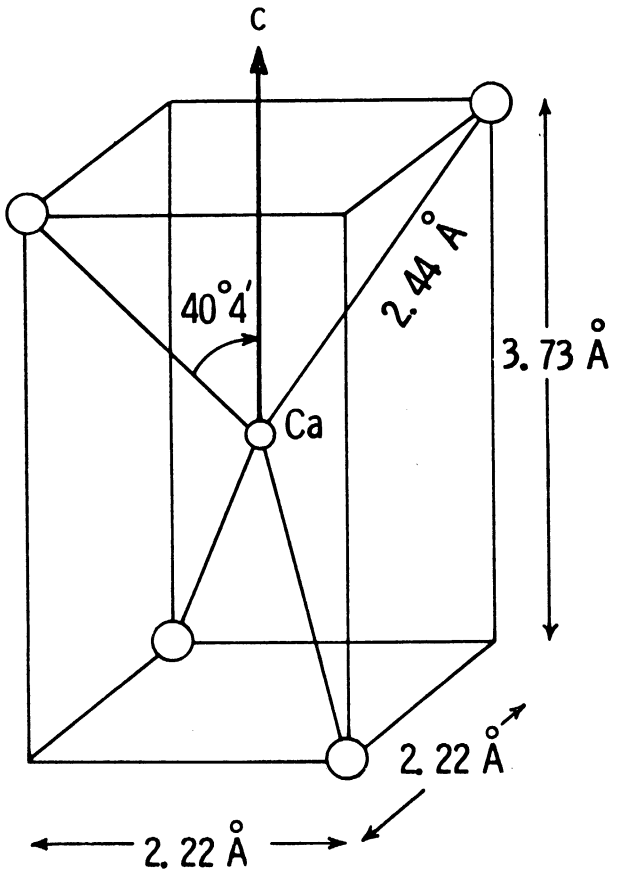

Figure 4(b). (Ca,O) "Long" and "Short" bond Bisphenoids.

radiation solid state physics. Kikuchi, Yip[25] and Chen explored systematically the usefulness of electron spin resonance as a tool for the study of radiation effects in solids and have compiled results and references up to the year of 1961. In this section only a brief description of electron spin resonance spectroscopy will be given. For texts on this subject one may consult Bersohn, Ingram, Pake, and Slichter as well as the reviews by Bleaney and Stevens, Bowers and Owen, and Jarrett.[26-32]

In the electron spin resonance experiment transitions are induced between the Zeeman levels of paramagnetic centers in the crystal. For the studies of radiation produced paramagnetic centers, the paramagnetism arises primarily from the unpaired electron spin angular momentum $\underline{S}$ and the associated magnetic moment. The electron spin resonance spectrum can be adequately described by the Hamiltonian

$$\mathcal{H} = \beta \underline{S} \cdot \underline{\underline{g}} \cdot \underline{H} + \underline{S} \cdot \underline{\underline{D}} \cdot \underline{S} + \sum_i \underline{S} \cdot \underline{\underline{A}} \cdot \underline{I}$$

The first is the Zeeman term. It expresses the interaction between the unpaired spin and the external magnetic field $\underline{H}$. The second term may be necessary for $\underline{S} > 1/2$ and is a measure of the distortion of the wavefunction by its surroundings. The last term is the hyperfine nuclear term and the summation is over each i-th nucleus in the vicinity of the center. By studying the electron spin resonance transitions as a function of crystalline orientation in the magnetic field, the principal values and axis orientations of the $\underline{\underline{g}}$, $\underline{\underline{D}}$ and $\underline{\underline{A}}$ tensors can be determined. This is the total information that one obtains from the measurement. The $\underline{\underline{g}}$ and $\underline{\underline{D}}$ tensors reflect information primarily about the overall character and symmetry of the paramagnetic center wavefunction

and its environment. The hyperfine tensor $\underline{\underline{A}}$ reflects the magnitude and symmetry of the unpaired electron wavefunction at the i-th nucleus, allowing a detailed mapping of the wavefunction over each of the atomic site neighboring the defect.

1.3 Uniaxially Stressed ESR (Electron Spin Resonance)

From the ESR study it is usually not possible to arrive at a unique model for the defect responsible for a spectrum. However, there are several ways of probing the defect which can aid greatly in the identification. Only the application of uniaxial stress will be mentioned here.

Many defects are anisotropic in the microscopic configuration. By anisotropic we mean that the defect has a lower order of symmetry than the host crystal. There is associated with such anisotropic defects an orientation degeneracy. That is the defect can occupy one of several equivalent orientations in the crystal. In equilibrium, statistically, an equal number of defects occupies each of the equivalent orientations, resulting in the macroscopic properties associated with these defects being isotropic. Under stress, the orientation degeneracy can be lifted i.e. the defects in the various orientations may no longer have the same energy. Consequently, provided the stress is applied to the crystal at a temperature at which the defects can reorient, a new distribution of defects among the various orientations will take place.

The use of stress induced alignment[33-38] in defects is, of course, not new. This has been the basis of internal friction experiments. In the case of uniaxially stressed ESR, defect alignment can be

studied directly. Each line in the ESR spectrum corresponds to one of the different orientations available to the defects. The integrated intensity under the peak is proportional to the number of defects in that direction. The stress induced alignment technique can be a powerful tool in studying such defect properties as symmetry and mobility and in correlating various properties associated with the same defect (e.g., an infrared absorption band and an ESR spectrum). This technique makes accessible defect information not obtainable from static measurements.

1.4 Radiation Damage Theory

The interaction of gamma-rays with matter occurs principally by means of three mechanisms: the photo-electric effect, the Compton effect and pair production. The passage of gamma-rays through a solid may thus cause extensive ionization and electron excitation which in turn lead to bond rupture, free radicals, coloration, and so forth, in many types of solids. There is also evidence that gamma-rays can produce displaced atoms in solids. Besides the effect of internal beta-ray bombardment and the direct recoils from gamma-ray events, two other possible mechanisms by which gamma-rays may produce atomic displacements have been suggested by Seitz and Varley.* Both of these mechanisms involve conversion of electron excitation energy to displacement energy and should be especially effective in insulators. In general the efficiency of atomic displacement by gamma-rays is quite low but occasionally detectable. In our case of niobium substituted in calcium tungstate, it will

---

* According to Dr. L. Chadderton the Varley mechanism does not work in computer simulation of radiation damage process.

be shown that Nb^{5+} becomes Nb^{4+} after gamma-ray irradiation. Since Nb^{4+} is paramagnetic it can be detected by ESR method.

Fast neutrons as bombarding particles produce radiation damage by direct collisions with nuclei. The prominent effect is atomic displacements. One of the fundamental problems in radiation damage is the determination of the number of defects formed in a substance by specified bombarding particles. Although most physical properties are altered by the presence of defects only a few are well enough understood to serve a quantitative measurement of the concentration of defects. It is interesting to note that with only few exceptions theoretical calculations of the number of displaced atoms have been constantly in disagreement with experimental results, and these few exceptions are where the direct method of measurement is available.[39] In addition to the electron spin resonance method used here there are two other direct methods of measuring the number of displaced atoms and both methods have provided results in good agreement with calculations. The first method uses the scattering of very slow neutrons by interstitials and vacancies to determine the defect concentration.[40] The second method uses optical absorption[39] measurement when the oscillator strength is known. In most cases where indirect methods are employed, theories predict a displacement yield five to ten times the observed amount. There are several possible explanations for the discrepancy. One possibility is that the interpretation of the experimental measurements is inaccurate. The relation between, say, change in resistance and number of interstitial-vacancy pairs may be inadequate. As will be shown later in this study calcium tungstate is an excellent material to check these possibilities. The fast neutron produced so called gamma-center

in calcium tungstate is identified as due to paramagnetic tungsten with a nearest oxygen displaced. Furthermore, it is found that the annealing at the irradiation temperature is very small. A measurement of the concentration of the gamma-centers therefore can provide a good check on radiation damage theory.[41-50]

There are two often cited theoretical treatments dealing with the problem of calculating the number of displacements produced by bombarding a substance with energetic particles such as fast neutrons due to Seitz-Koehler and Kinchin-Pease. Their similarities and differences have been discussed by Dienes and Vineyard.[41] In the low energy region ($E \sim E_d$). these two theoretical results differ considerably. For high energy bombarding particles such as fast neutrons, these two theories provide approximately the same results. In most cases the Kinchin-Pease treatment predicts that approximately 20 percent less defects are produced for the same energy of fast neutrons than the Seitz-Koehler treatment. The Kinchin-Pease theory is easier to handle computationally and will be used here.

Fast neutrons produce defects through the production of primary knock-ons which in turn create additional (secondary) knock-ons while dissipating their recoil energies in the solid. For fast neutrons with energy E' as bombarding particles the collisions are of the hard sphere type. Only a small portion of the struck atoms are not displaced and, therefore, the cross section for producing a primary knock-on can be assumed to be the total neutron scattering cross section. To determine the expected number of displacements per scattered fast neutron Kinchin and Pease treatment gives the following relations

$$\nu(E) = 1 \qquad E_p < E_d$$

$$\nu(E) = E_p / 2E_d \qquad 2E_d < E_p < E_i$$

$$\nu(E) = E_i / 2E_d \qquad E_p > E_i$$

where E_p is the energy of the primary knock-on

E_d is the threshold energy for displacement and

E_i is the limiting energy for ionization.

In most investigations including the Kinchin-Pease treatment, a model is chosen in which the atoms in a lattice have a sharp threshold energy E_d for displacement. That is, if a lattice atom recieves an energy greater than E_d it is displaced; whereas if it receives an energy less than E_d it remains at its site and dissipates the acquired energy through lattice vibrations. This model is, of course, not a true picture of the situation but it has been used because it is simple and accurate enough for most discussions. It is more realistic to suppose that the displacement threshold energy is not sharp, but there is some probability that a lattice atom which gains energy E will be displaced. There are several reasons why the threshold energy is not sharp. One reason is that the energy required to free an atom will depend upon the crystallographic direction. It is surely harder (requires more energy) for an atom to leave its lattice site if the atom is initially directed toward one of its nearest neighbors than it is initially directed toward the center of the triangle formed by three nearest neighbors. Another reason is that the degree of the thermal vibration in the neighborhood of the struck atom will influence the amount of energy necessary to displace the atom.

However the sharp threshold model is applicable in many cases if it is used with caution. The concept of an effective sharp threshold energy of displacement has been critically studied by several investigators. Using different displacement probability functions Hurwitz and Lehmann[51] have shown that the sharp threshold assumption gives acceptable results as long as the energy region over which the displacement probability function is rising from zero to unity is small in comparison with the kinetic energy of the primary of interest. Fein[52] used a model for the displacement of atoms in which each atom of a crystal has a threshold energy that is a random variable and shown that for moderately large energies of the bombarding particles the physical effects of bombardment by either neutrons or charged particles can be pictured as arising from an effective sharp threshold energy and that this effective threshold is the same for both types of bombardment. From the results of these investigations, it seems that the model of an effective sharp threshold displacement energy is meaningful and applicable in the case of fast neutron bombardment.

The limiting energy for ionization E_i is defined such that when the moving atom, having energy E less than E_i, will not lose energy to an appreciable extent by ionization and such that when E is much greater than E_i the ionization loss will greatly exceed that due to elastic collisions. In estimating E_i it is usually assumed that if the velocity of the moving particle is slow compared to the slowest orbiting atomic electron, the electron may relax without excitation, whereas excitation becomes more probable as the velocity of the moving particle becomes comparable to or greater than that of the slowest

electron. This reasoning led Seitz to suggest that for insulators such as calcium tungstate

$$E_i = \frac{1}{8}\left(\frac{M}{M_e}\right) E_L$$

where M is the mass of the primary

M_e is the mass of the electron

E_L is the lowest electronic excitation energy given by the low energy limit of the main optical absorption band.

E_L for calcium tungstate has been measured by R. H. Gillete[14] and K. Nassau.[16] It varies from 0.25 to 0.30 microns depending on the history of the crystals. Using a Cary-11 dual beam spectrophotometer the low energy limit of the main optical absorption band of the crystals used in this study has been measured as 0.25 microns. This gives the limiting ionization potentials as follows:

$$E_i(O) = 18 \text{ kev}$$

$$E_i(Ca) = 45 \text{ kev}$$

$$E_i(W) = 209 \text{ kev}$$

Questions have also been raised about the usefulness and validity of the concept of average number of displacements per primary collision. The fundamental question is what the statistical fluctuation will be. If the fluctuation is large the concept of average number per collision will be less useful. Using the Kinchin-Pease model and assuming hard sphere scattering Leibfried[48,53] has shown that

$$S = \frac{\bar{\nu}^2 - \bar{\nu}^2}{\bar{\nu}^2} = \frac{0.15}{\bar{\nu}} \qquad \text{for} \quad \nu \geq 2$$

Lehmann[51] has further extended this study. Considering both the Kinchin-Pease and Seitz-Koehler models and different scattering laws he proved that the statistical fluctuation is small in all cases for moderately large bombarding particle energy. In the case of reactor fast neutron bombardment, a sharp value of the average number of displacements per primary collision will be permissible.

The Kinchin-Pease treatment is for the case of monatomic solids. The influence of different masses of diatomic solids on the displacement cascade has been investigated by Baroody.[54] Consider a diatomic solid of type AB in which the probabilities for collisions involving various pairs of atoms are equal. Suppose that a primary knock on with $\frac{E}{E_d} = y > 2$ is produced and let $N_1(y)$ and $N_2(y)$ be the numbers of atoms like and unlike the primary, respectively, which are finally displaced. Baroody reached the following result. For large value of y

$$f(y) = N_1(y) - N_2(y) \doteq B(\lambda) + C(\lambda)\left(\frac{y}{2}\right)^{\alpha}$$

where

$$B(\lambda) = \frac{2\lambda - (1-\lambda)\epsilon_1 - \lambda\epsilon_2}{2\lambda + (1-\lambda)\ln(1-\lambda) + \lambda \ln \lambda},$$

$$\alpha C(\lambda)\left[2\lambda + (1-\lambda)^{\alpha+1} \ln(1-\lambda) + \lambda^{\alpha+1} \ln \lambda\right]$$

$$= \lambda\left[1 - (2\lambda)^{\alpha}\right] \qquad \lambda \leqslant \frac{1}{2}$$

$$= (1-\lambda)\left\{1 - \left[2(1-\lambda)\right]^{\alpha}\right\} \qquad \lambda > \frac{1}{2}$$

and $$\lambda = \frac{4 M_A M_B}{(M_A + M_B)^2}$$

α is the nonzero root of s of the equation

$$2\lambda s - 1 + (1-\lambda)^{s+1} + \lambda^{s+1} = 0$$

and ϵ_1 is the smaller of $-\ln(1-\lambda)$ and $\ln 2$, and ϵ_2 is the smaller of $-\ln\lambda$ and $\ln 2$. The result is clearer when one plots $N_2/(N_1+N_2)$ against λ for different values of y as shown in Figure 5. For $y = 1{,}000$ and larger the fraction $N_2/(N_1+N_2)$ is practically equal to 0.5 for λ varying from 0.3 to 1. In our case of fast reactor neutron irradiation, the displacements due to neutrons with energy less than 25kev contributes less than one percent of the total displacements, therefore the effect of mass difference is of little importance.

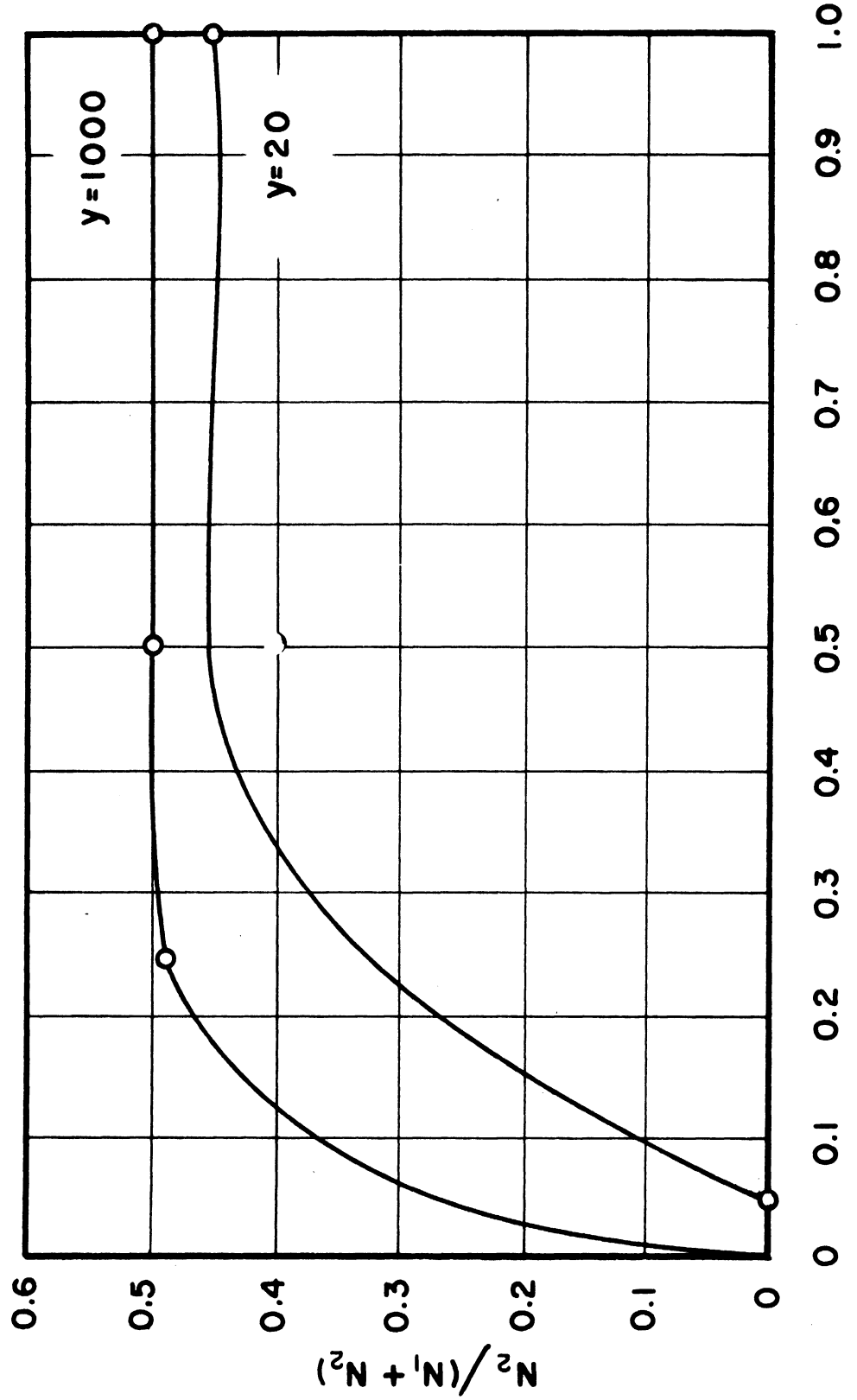

Figure 5. Mass Dependence of Fractional Displacement.

2. EXPERIMENTAL PROCEDURE

2.1 Samples and Orientations

Samples investigated were calcium tungstate single crystals grown at Harry Diamond Laboratories* by the Czochralski method. Most unirradiated crystals showed prominent spectrum of Mn^{++}, although the impurity content of different crystals varied by as much as a factor of ten. Crystals were oriented by X-ray diffraction and cemented to the end of quartz rods. Back reflection Laue patterns with X-ray beam parallel to the [110] and [001] axes are shown in Figure 6 and Figure 7. The mounted crystals were then inserted into the microwave cavities at right angles to the steady magnetic field. The quartz rod served as the rotational axis for changing the crystal orientations.

2.2 Electron Spin Resonance Measurements

ESR measurements were made by using an X-band spectrometer (9.5 Gc/sec) with 5kc/sec modulation and a Ku-band spectrometer (16.5 Gc/sec) with 400c/sec modulation. Ceramic cylindrical TE-011 cavities with variable cross coupling loops were used for both room temperature and liquid nitrogen temperature measurements. A 12 inch Varian rotating electromagnet with 3.25 inches gap provided the magnetic field. Magnetic fields were measured by using a F-8 fluxmeter connected to a Berkeley 7800 transfer oscillator and a Berkeley 7370 Universal EPUT.

2.3 Irradiations

Nuclear reactor irradiations were made in the University of Michigan swimming-pool type research reactor. Samples were placed in

---

* We would like to thank Mr. W. Viehmann for his generous supply of crystals.

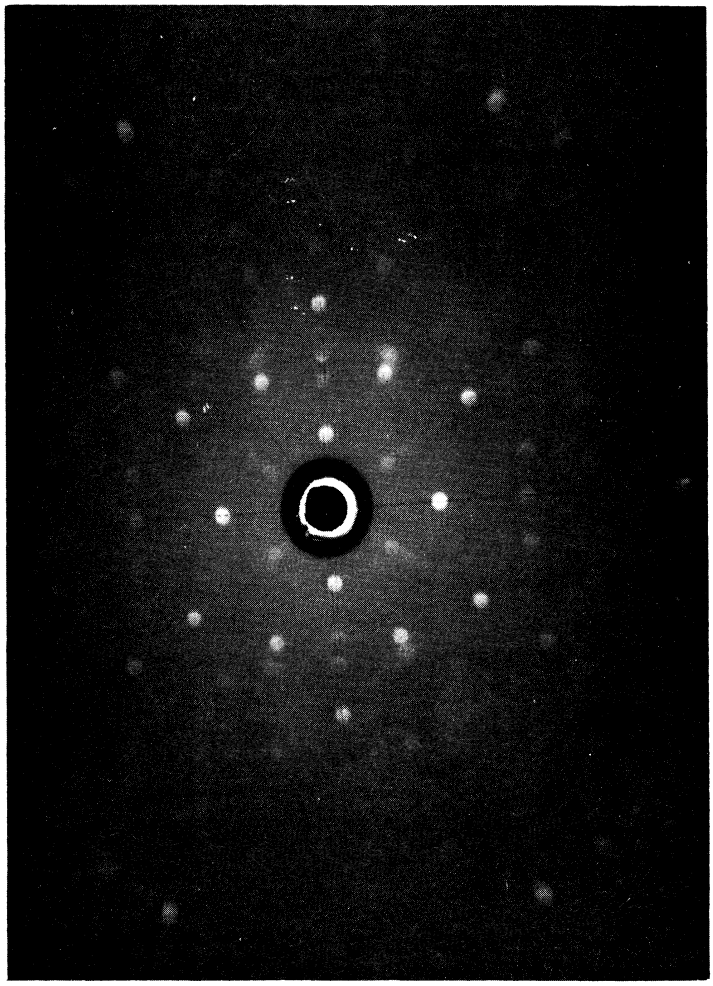

Figure 6. Back Reflection Laue Pattern of Calcium Tungstate Crystal with X-Ray Beam Parallel to the [110] Axis.

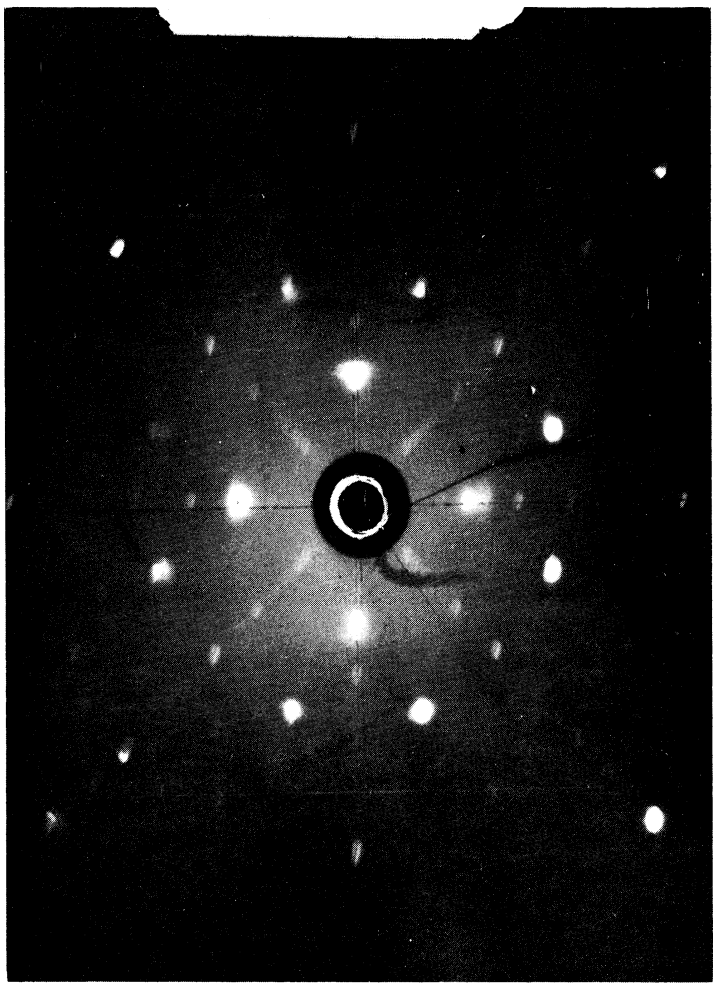

Figure 7. Back Reflection Laue Pattern of Calcium Tungstate Crystal with X-Ray Beam Parallel to the [001] Axis.

a small polyethylene bottle using bismuth as weights. In order to maximize the fast neutron flux, irradiations were conducted at a location close to the reactor core where the temperature was approximately 60°C estimated from the coolant temperature. The fast and thermal fluxes were 10^{13} and 10^{12} n/sec-cm^2 respectively. Irradiation times from 20 minutes up to 20 hours were used. A longer irradiation time was not feasible due to excessive induced radioactivity of tungsten W^{185} and W^{187}. Since the observed effects were due to fast neutrons, most irradiations were done with the samples wrapped in cadimum cylinder of 30 mil thickness to minimize excessive induced radioactivity due to thermal neutrons.

After irradiation, samples were removed from the reactor core region and left at the side of the pool where the neutron flux is negligible for a period from three to fifteen days depending on the irradiation time.

Gamma irradiations were made with a calibrated 10,000 curie Co^{60} source. X-ray irradiations were made using a GE X-ray unit with a tungsten tube operating at 50 kvp and 50 ma, both at the Phoenix Laboratory of the University of Michigan.

2.4 Uniaxial Stress

Uniaxial stress was applied to the sample up to 11,000 psi. The sample was placed on a Teflon cylinder which becomes hard at low temperature. A simple lever with weight outside the Dewars supplied the force to the quartz rod and on the other end of the quartz rod the oriented sample was cemented. A diagram of the uniaxial stress apparatus is shown in Figure 8.

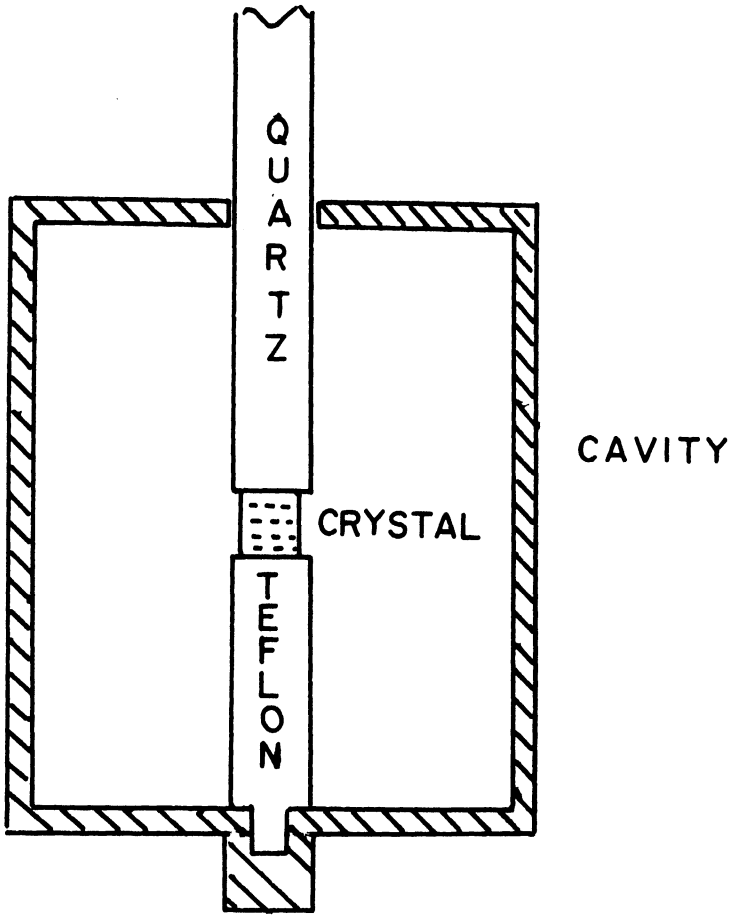

Figure 8. Uniaxial Stress Cavity.

2.5 Neutron Flux Measurement

Many earlier radiation effect experiments have been conducted without precisely measured neutron flux data. For some work the neutron flux was reported in integrated units with an estimated mean energy value of the neutron spectrum. It was claimed that in the case of light elements when the mean neutron energy is much larger than the limiting ionization energy E_i, the lack of precise neutron flux data would not introduce much uncertainty. Since tungsten is a heavy element, the precise neutron flux data is indispensible for the calculation of the number of defects.

Fast neutron flux up to 12 Mev at the University of Michigan Ford Nuclear Reactor has been measured by Harris, Sherwood and King[55] using a solid state proton recoil fast neutron telescope. At the location two inches away from the reactor core in the median plane of the core, the differential fast neutron flux is as follows:

Energy (Mev)	n/cm-sec-Mev x 10^{11}
1	2.80
2	2.73
3	2.21
4	1.19
5	.88
6	.46
7	.25
8	.13
9	.07
10	.03
11	< .01

The thermal neutron flux and epithermal neutron flux measurement were made using the gold foil activation technique. Gold was used because of its appropriate half life and large activation cross section. Both bare and 30 mil thick cadmium covered gold foils were used. The foils were weighed on an electrobalance before activation. The activation of the irradiated gold foils was determined using a well counter in conjunction with a multichannel analyzer. The thermal neutron flux was determined from the measured activity of the irradiated gold foil using the relationship

$$\Phi_{th} = \frac{R_b - R_c}{\epsilon N_D \langle \sigma_a \rangle}$$

where Φ_{th} is the thermal neutron flux, R_b and R_c are the rates of production of radioactive nuclei in the bare and cadmium covered gold foils respectively. ϵ is a correction factor for the flux depression. N_D is the total number of atoms in the detector and $\langle \sigma_a \rangle$ is the microscopic absorption cross section averaged over the Maxwell-Boltzmann distribution. The rate of production of radioactive nuclei for the bare and cadmium covered foils is given by

$$R = \frac{C/f}{(1 - e^{-\lambda \tau})\, e^{-\lambda t}}$$

where C is the specific activity of the gold corrected for the background, f is the efficiency of the counting system, λ is the decay constant, τ is the duration of the irradiation, and t is the time lapse between irradiation and counting. No correction for the change in activity during measurement was made because the half life of gold is 2.7 days compared to the counting time of two minutes. The

fuel elements of the Ford Nuclear Reactor are essentially the same as that of the Bulk Shielding Reactor. For BSR the neutron flux at the location about two inches away from the reactor core in the median plane of the core has been measured by Trice.[56] The neutron flux was found 1/E up to 50kev. In a 1/E spectrum the measurement of k is thus sufficient for the whole energy range where $\Phi = k/E$ is valid. The ratio R_{cd} is determined from the cadmium ratio defined by

$$R_{cd} = \frac{R_b}{R_c}$$

The neutron energy spectrum used for the calculation of the number of oxygen vacancies is shown in Figure 9, where epithermal neutron flux up to 0.5 Mev is assumed to be 1/E and is determined by gold foil activation, and fast neutron flux is quoted from Reference 55.

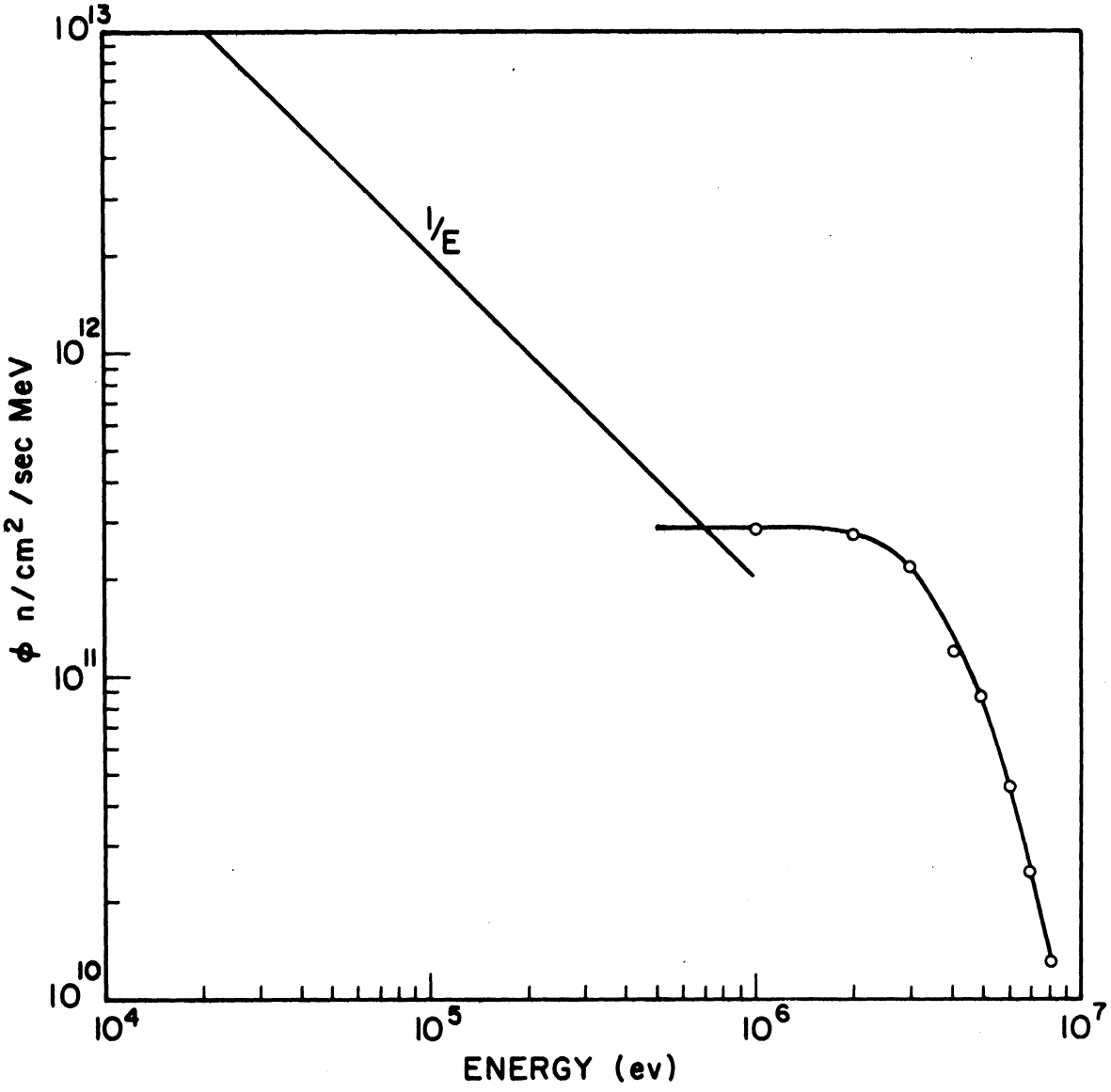

Figure 9. Neutron Flux Spectrum at the Irradiation Facility.

3. EXPERIMENTAL RESULTS AND DISCUSSIONS- PARAMAGNETIC TUNGSTEN(57)

ESR spectrum of reactor irradiated calcium tungstate single crystals were studied at microwave frequencies of 9.5 Gc/sec (X-band) and 15.5 Gc/sec (Ku-band). The spectrum at liquid nitrogen temperature for the magnetic field H parallel to [001] and [110] directions are shown in Figure 10 and Figure 11 respectively. Before irradiation the ESR spectrum observed is identified as due to unintended Mn^{++} impurities. After reactor irradiation new groups of lines are observed at room temperature and liquid nitrogen temperature. From the angular dependence of the spectrum new lines are classified into three groups and will be referred to as the α-group, the β-group and the γ-group respectively. Irradiation at room temperature with Co^{60} gamma rays or 50 kvp X-rays up to 10^7 rads did not produce new ESR lines in agreement with Zeldes and Livingston.(58) By comparison the results of bare samples and samples covered with 30 mil cadmium sheet during irradiation the new groups of lines are found due to fast neutrons.

The α-group is the only one which can be observed at room temperature. Its g-value varies from 2.005 to 2.033. No hyperfine interaction of tungsten isotope W^{183} is observed and the angular dependence of this group of lines cannot be correlated with the crystal structure and is the least understood. From the intensity consideration it is tentatively assigned to oxygen interstials. The β-group and the γ-group are observed at liquid nitrogen temperature. Both have hyperfine lines attributable to tungsten W^{183}. From the angular variation of the spectrum the α-group is identified as due to paramagnetic tungsten

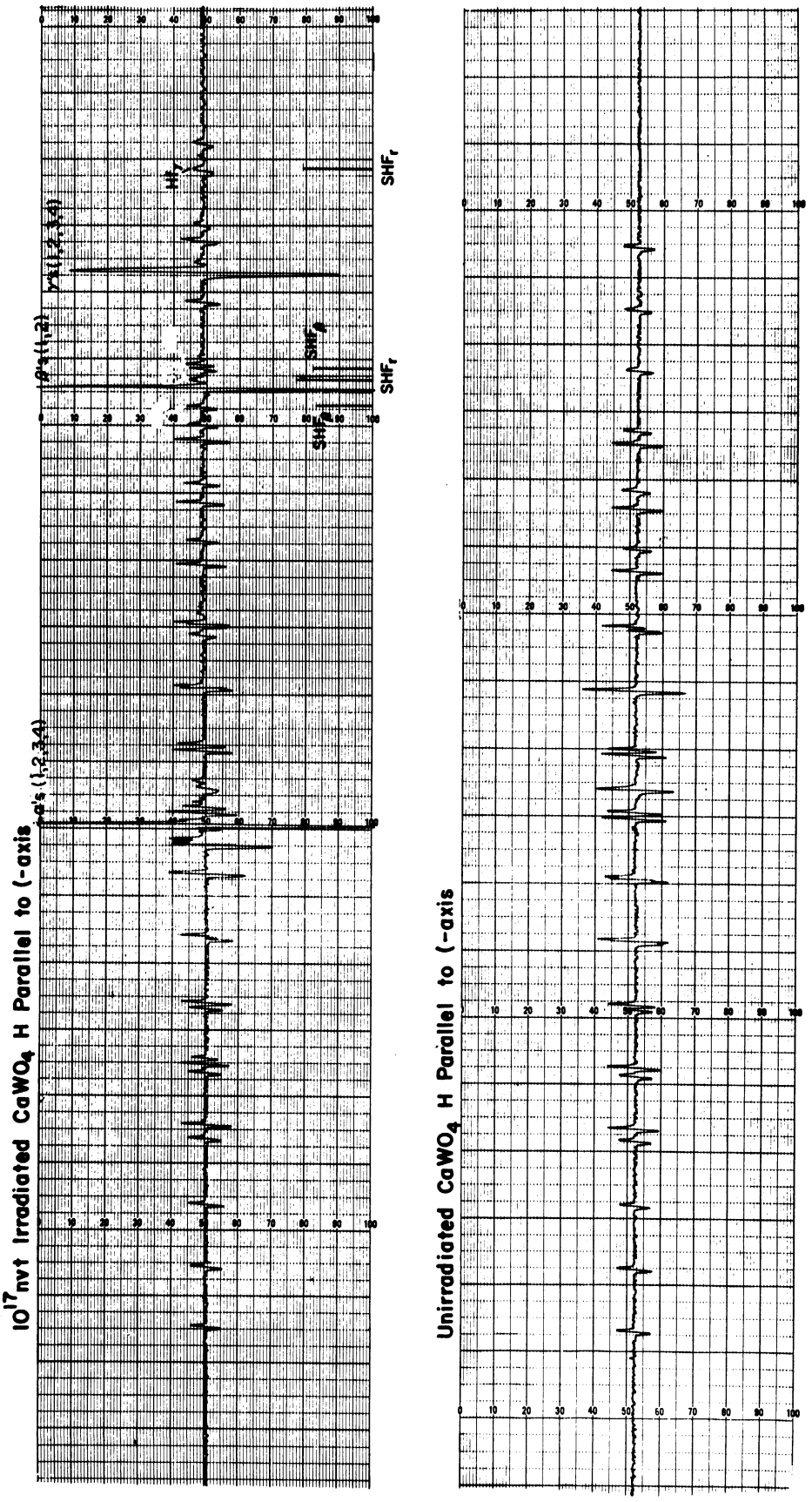

Figure 10. ESR Spectrum of 10^{17} nvt Reactor Neutron Irradiated Calcium Tungstate, H Parallel to the [001] Axis.

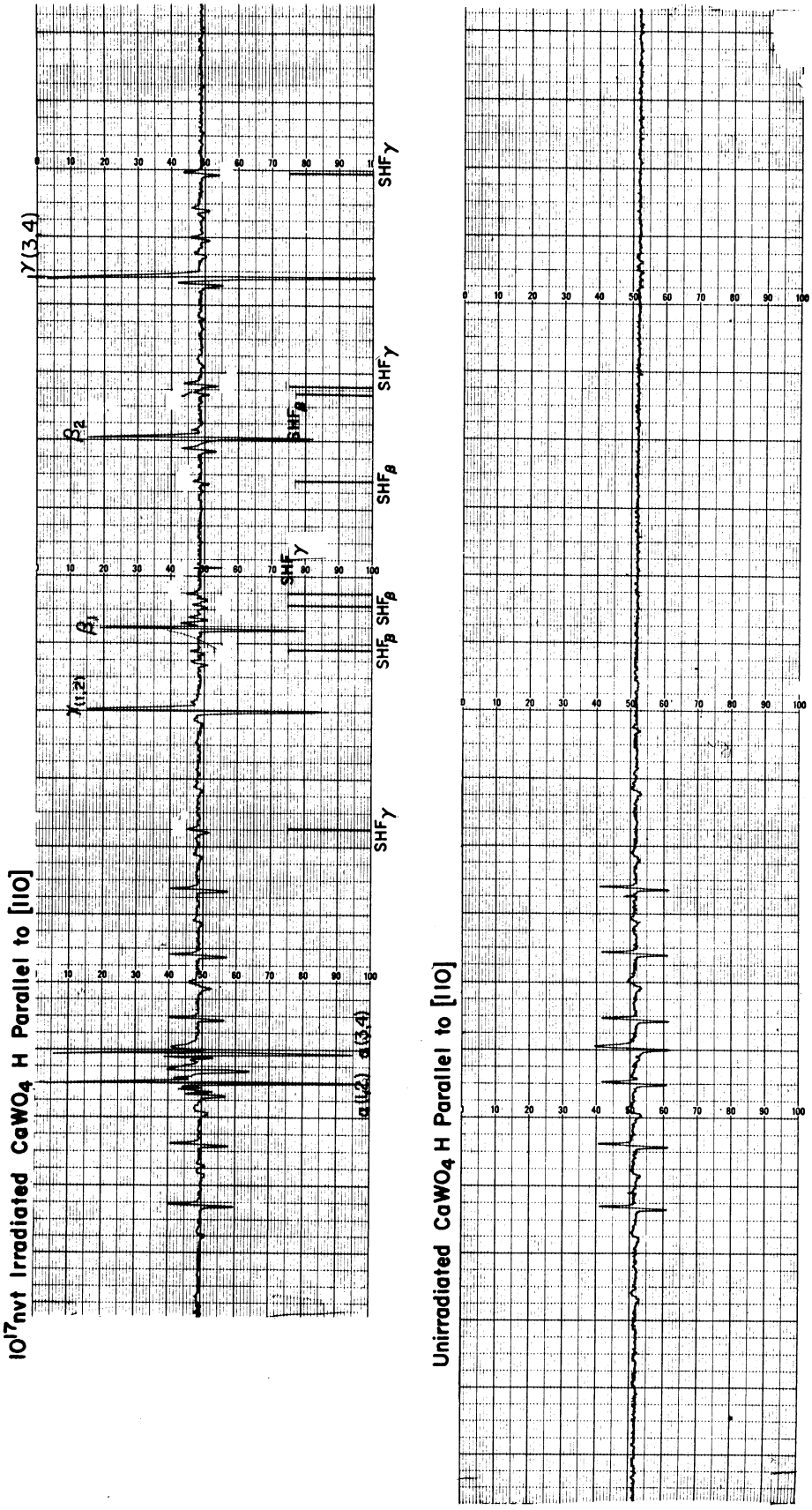

Figure 11. ESR Spectrum of 10^{17} nvt Reactor Neutron Irradiated Calcium Tungstate, H Parallel to the [110] Axis.

with a nearest oxygen vacancy. Uniaxial stress experiment provides further support for these assignments. The α- and γ-groups are very stable at room temperature but the β-group decays slightly. All three groups can be annealed out by heating at 600°C for an hour. The concentration of the γ-group is measured and compared with the predictions of the Kinchin-Pease theory.

TABLE I

THE PRINCIPAL VALUES OF THE g-TENSORS AND THE DIRECTIONS OF THE AXES OF THE GAMMA CENTER

	z	x	y
g	1.914	1.675	1.646
Δg	0.088	0.327	0.356
θ_1, θ_2	57°	147°	90°
φ_1	32°	32°	302°
φ_2	212°	212°	112°
θ_3, θ_4	123°	33°	90°
φ_3	302°	302°	32°
φ_4	122°	122°	212°

3.1 Electron Spin Resonance

a. The Gamma-Group

Most of the measurements are made with samples irradiated in reactor for an hour (10^{17} nvt fast neutron dosage). The spectrum is shown in Figure 10 and 11. The γ-group can only be observed at liquid

nitrogen temperature. In general it consists of four central lines of equal intensity and each central line is flanked by two satellites. The intensity ratio of the central line and the satellite is about twelve to one and this is interpreted as due to nuclear hyperfine interaction of the tungsten isotope W^{183}. The hyperfine interaction is anisotropic varying from 280 to 320 gauss. Along crystal c-axis the four sets of lines merge into one set at $g = 1.75$. In the (001) plane only two sets of lines are observed. The angular variations of the γ-group when the magnetic field is varied in (001) and (110) planes are shown in Figure 12 and Figure 13 respectively.

Both maximum and minimum g-values of the gamma lines occur when the magnetic field is varied in the diagonal plane of the squashed tetrahedron formed by the oxygens of the tungstate. This gives the measured components of the g-tensors and the directions of the principal axes as shown in Figure 14 and Table I.

It is interesting to note that the four g_z's are within experimental error along the four tungsten oxygen bonds of the tungstate. More specifically as shown in Figure 14, when g_z is parallel to $W\text{-}O_2$, g_y is found along the normal to the plane of $O_1\text{-}W\text{-}O_2$, and g_x is found perpendicular to both g_z and g_y. In other words the symmetry of this paramagnetic center is in good agreement with the model of paramagnetic tungstate with a single disturbed tungsten-oxygen bond. The four orientations of the disturbed tungsten-oxygen bond directions provide four different sites of the center. Along the crystal c-axis all four orientations are equivalent and the spectrum merges into a single set. In the (001) plane the four orientations become equivalent in pairs and only two sets of lines are observed as evidenced in Figure 12.

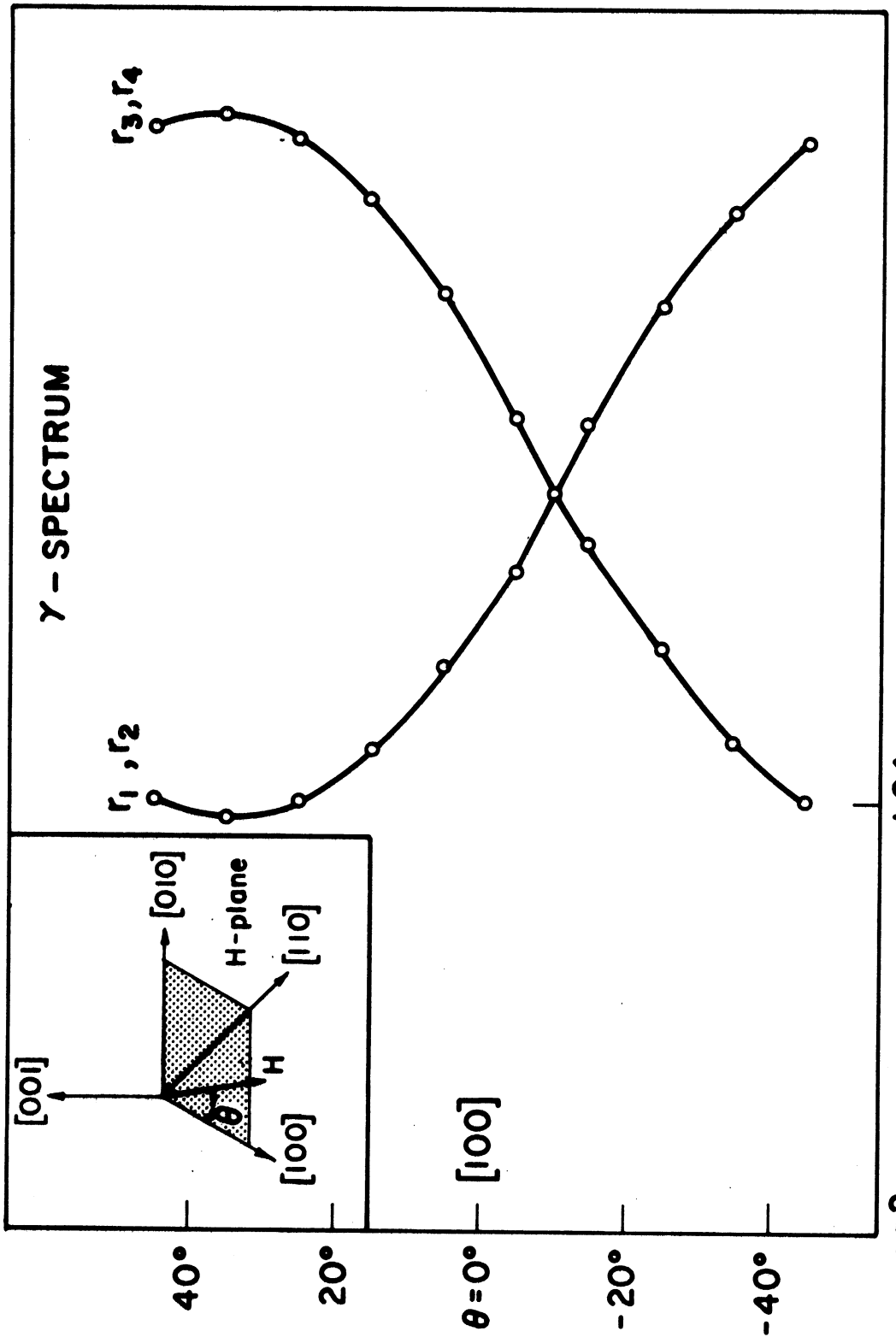

Figure 12. Angular Variation of the γ-spectrum, H in the (001) Plane.

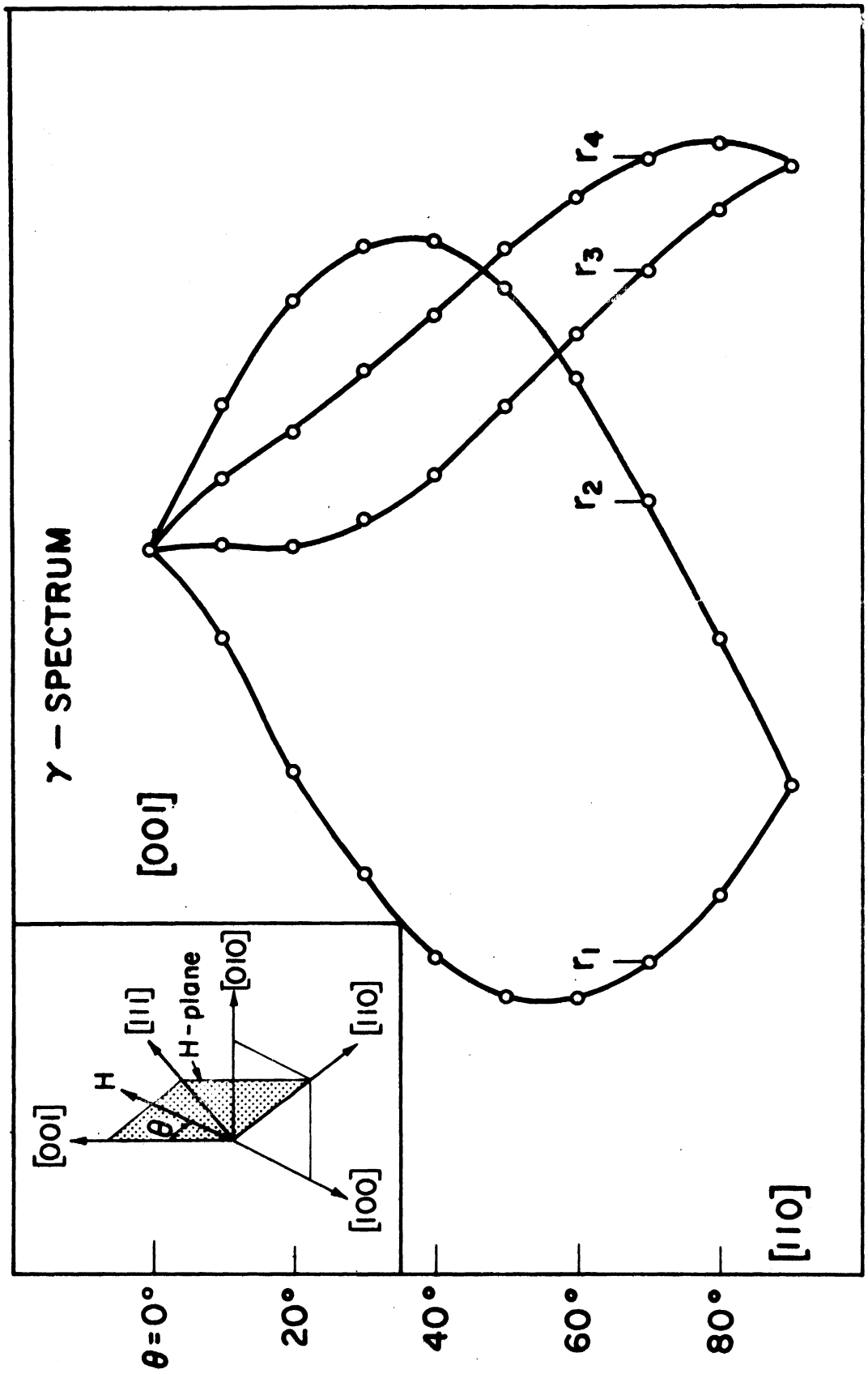

Figure 13. Angular Variation of the γ-spectrum, H in the (110) Plane.

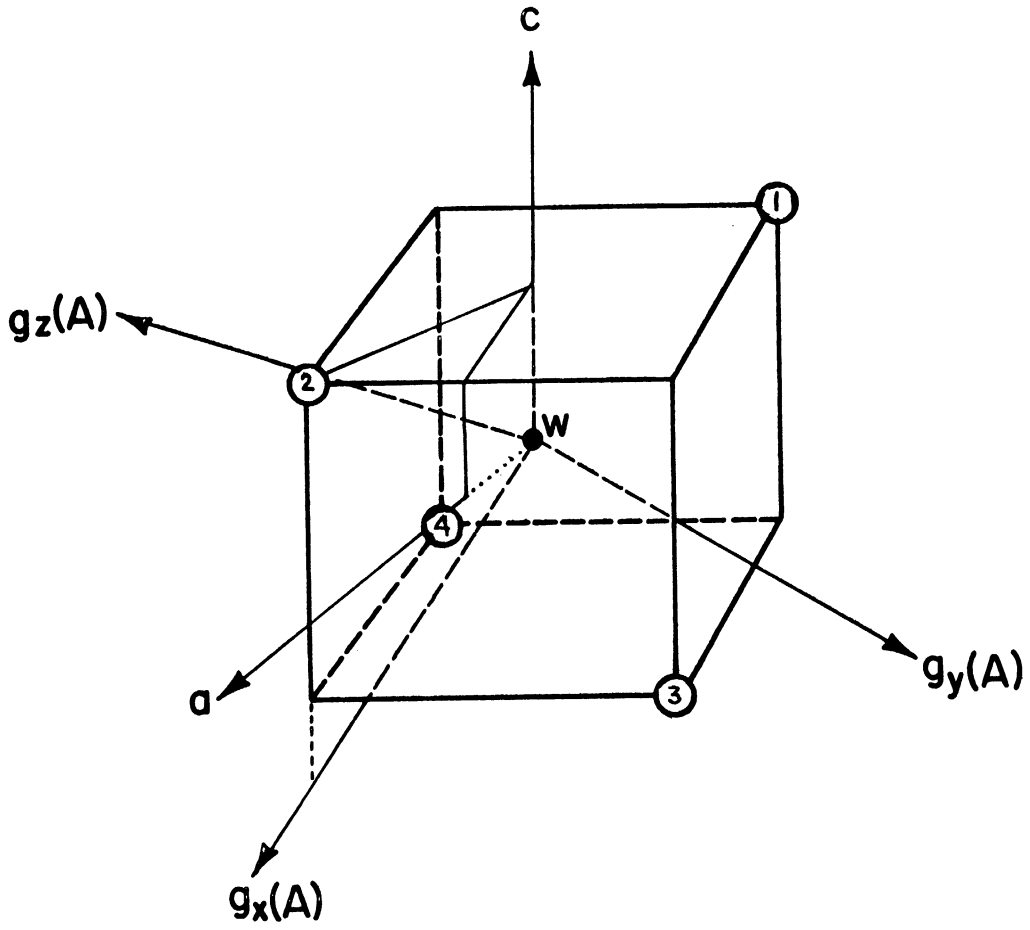

Figure 14. g-tensor of the γ-center.

In order to test the model of paramagnetic tungstate with a disturbed tungsten-oxygen bond, further measurements have been made. The crystal was first oriented and mounted along one of the tungsten-oxygen bond direction and the magnetic field was varied in a plane normal to this bond direction. As shown in Figure 15 one of the gamma lines, namely, r_4 was found to be almost independent of the magnetic field and the remaining three vary with a period of approximately 120 degrees. This is what is expected from the model. r_4 is due to centers whose g_x and g_y axes are in the H-plane, since g is very close to g, the line position changes very little with the magnetic field. The remaining three lines are due to centers which form approximately an equilateral triangle in the H-plane. Their line positions therefore vary with a period of approximately 120 degrees.

As a further check, the magnetic field was varied in the diagonal plane of the squashed tetrahedron formed by the four oxygens of the tungstate. For this case two of the tungsten-oxygen bond directions become equivalent. This is evidenced by the three line spectrum as shown in Figure 16. Furthermore, the intensity of line-r_3 r_4 is twice as the remaining two, namely, r_1 or r_2.

The observed g-values can be accounted for qualitatively by assuming an unpaired 5d electron of the tungsten subject to the crystalline electric field of three nearest oxygens of the prominently C_{3v} symmetry and a small C_s symmetry distortion. The details of the analysis are given in the Appendix. The calculation suggests that $|\Delta g_z| < |\Delta g_x| \sim |\Delta g_y|$ where $\Delta g_i = g_i - g_e$ and g_e is the spectroscopic splitting factor of free electron. This is in agreement with the experimental results.

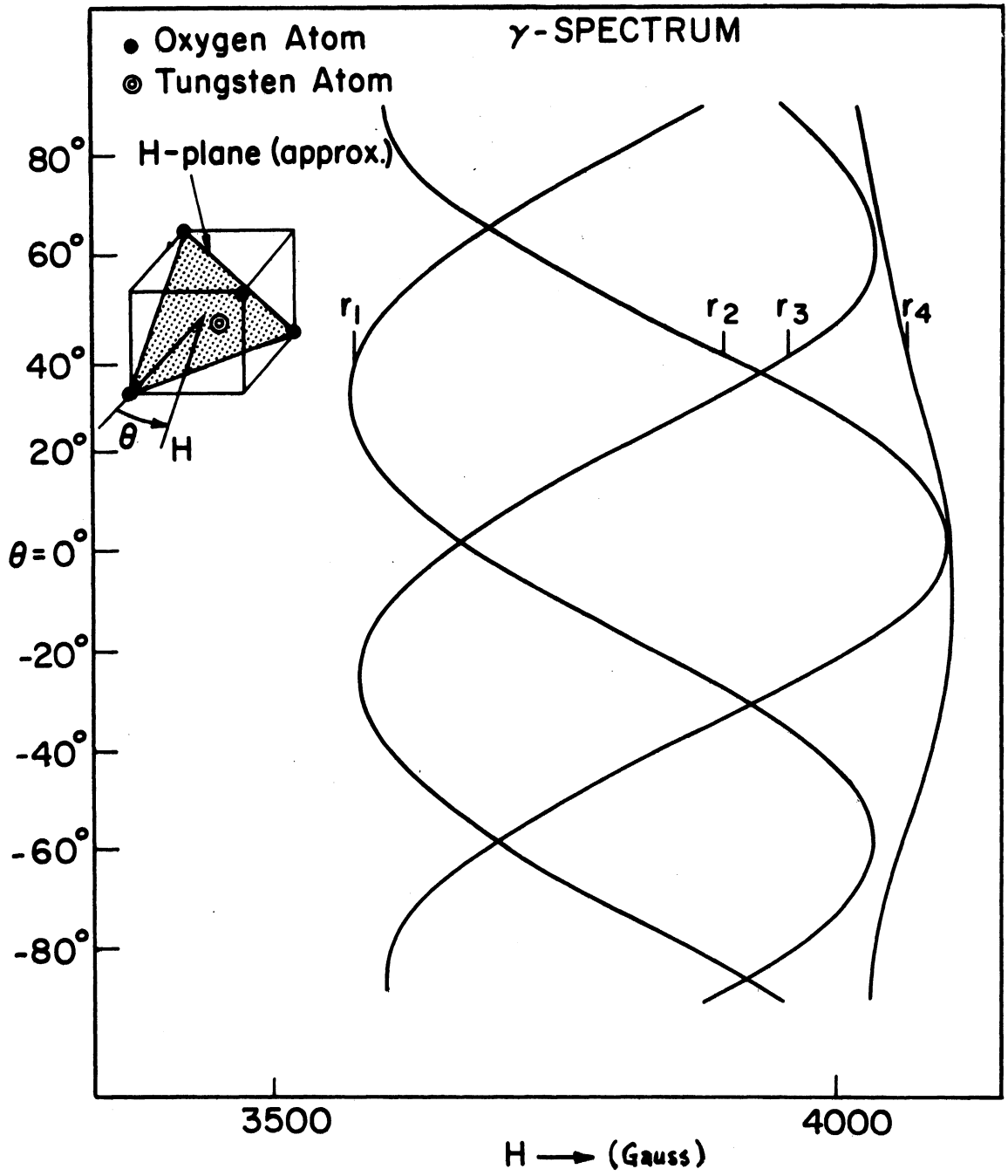

Figure 15. Angular Variation of the γ-spectrum, H Perpendicular to the W-O Bond Direction.

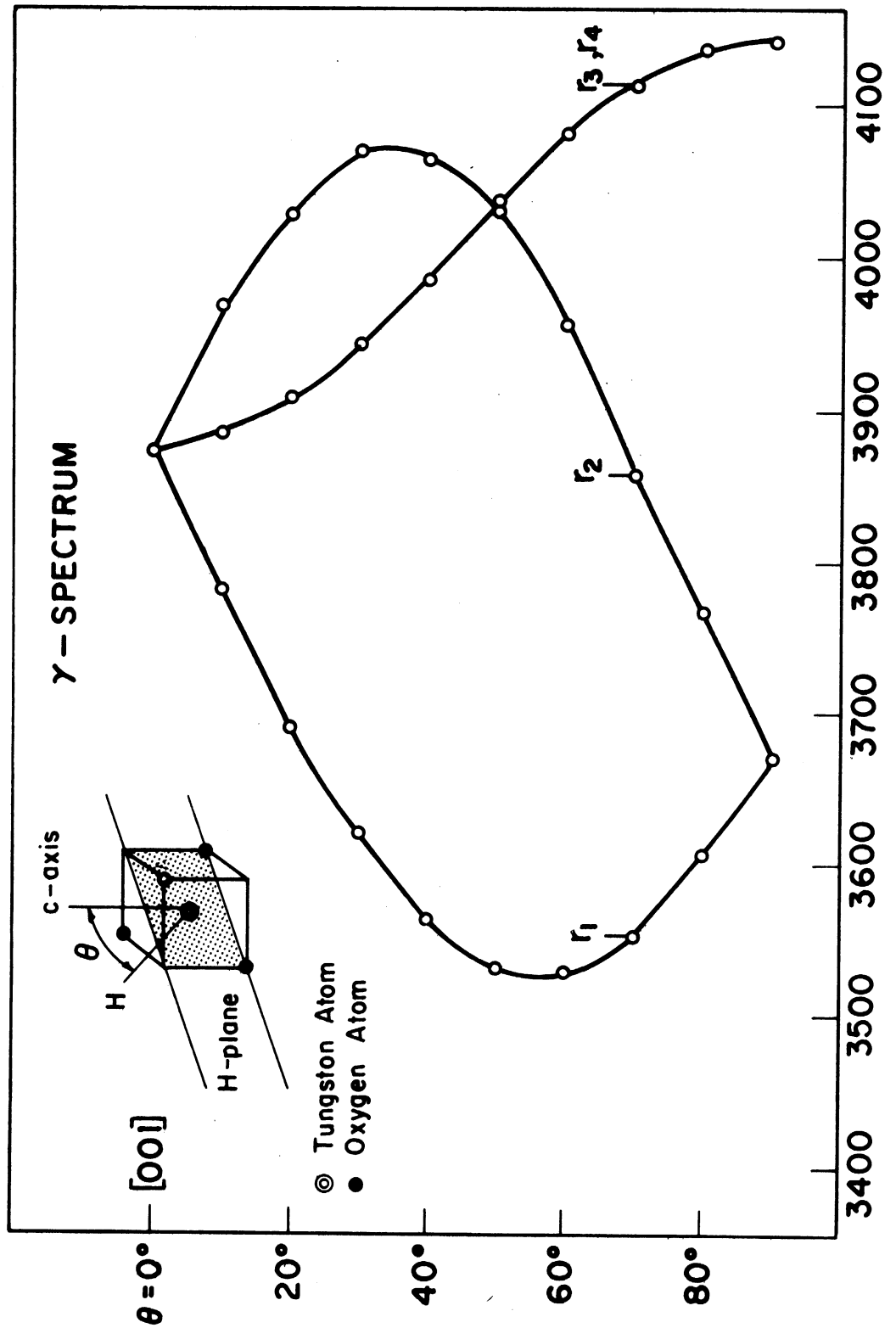

Figure 16. Angular Variation of the γ-spectrum, H in the Diagonal Plane of the WO_4 Bisphenoid.

The gamma-center is very stable at room temperature. No measurable change is found for a period of four weeks. Heating up to 60°C which is about the temperature during reactor irradiation does not give any measurable effect. Heating up to 600°C for an hour completely anneals out the gamma-spectrum.

The hyperfine separation of 280 gauss along the crystal c-axis and 320 gauss along [110] direction seems unusually large considering the small magnetic moment of W^{183} (0.115 nuclear magneton). The large isotropic part of hyperfine interaction observed implies that the 6S state must have significant contribution. The Fermi contact term effective fields H_c as obtained from experiment for various alkali atoms is shown as follows:(59)

Atom	Hc (in kilogauss)
Li	122
Na	394
K	581
Rb	1229
Cs	1513

The rapid and monotonic increase of H_c from Li to Cs provides an indication that the large observed hyperfine interaction is not unreasonable.

b. The β-group

The β-group can only be observed at liquid nitrogen temperature (77°K). The angular dependence of the beta-lines when the magnetic field is varied in the (001) and (110) planes is shown in Figure 17 and Figure 18.

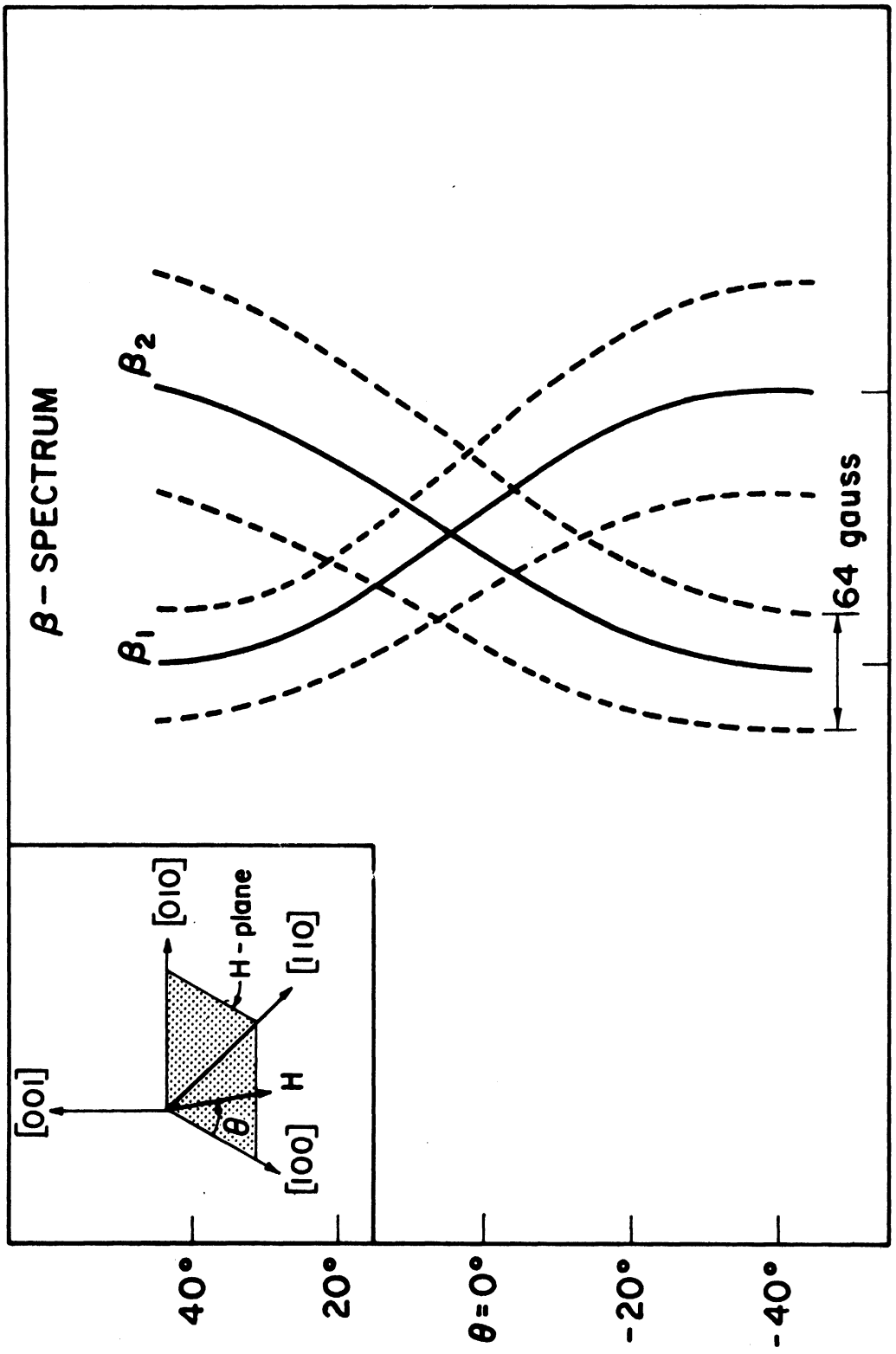

Figure 17. Angular Variation of the β-spectrum, H in the (001) Plane.

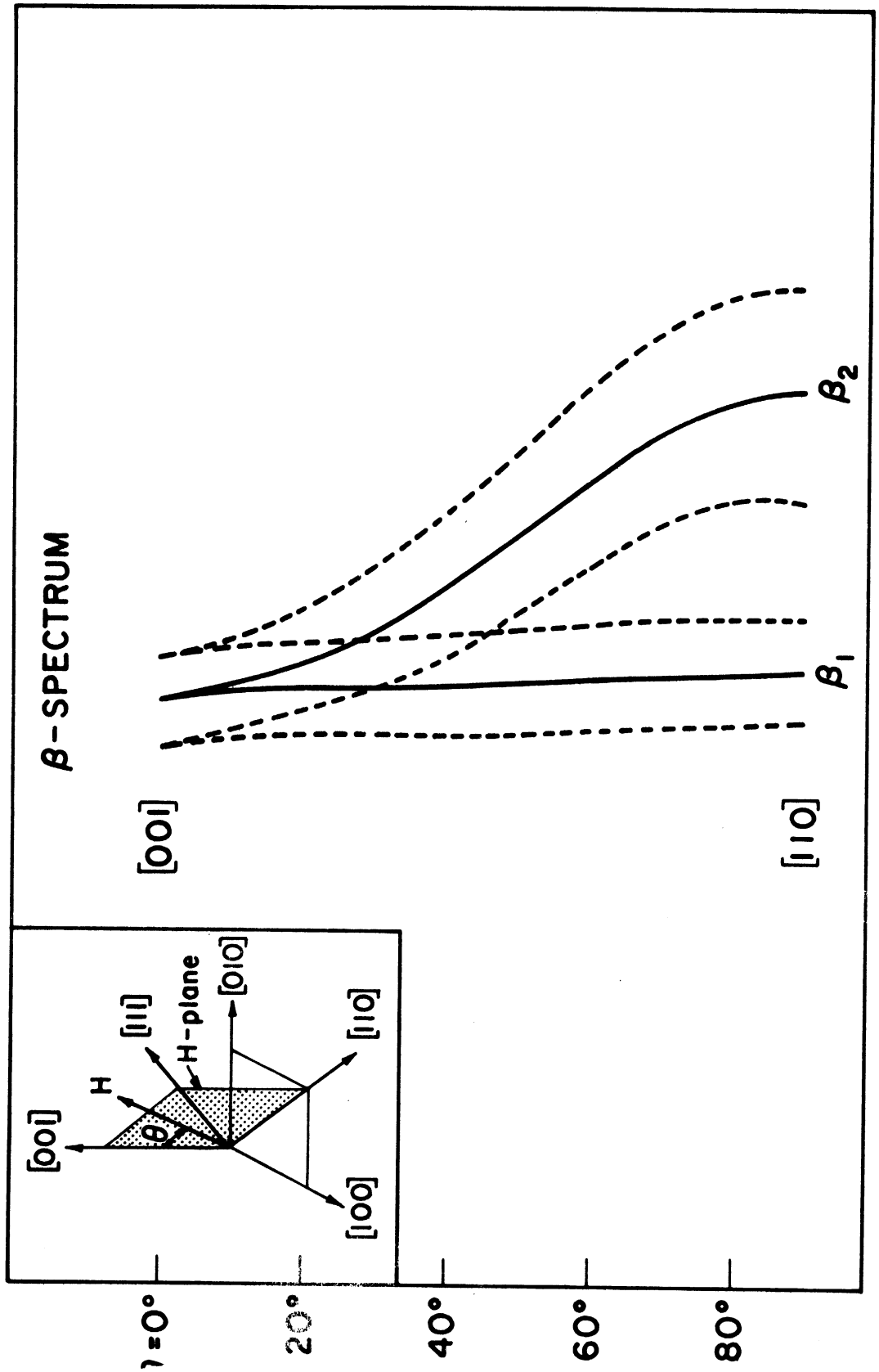

Figure 18. Angular Variation of the β-spectrum, H in the (110) Plane.

TABLE II

THE PRINCIPAL VALUES OF THE g-TENSORS AND THE DIRECTIONS OF THE AXES OF THE β-CENTER

$g_z = 1.81$	$g_x = 1.791$	$g_y = 1.724$
θ	90°	90°
φ_1	44°	134°
φ_2	134°	44°

θ is the angle between each tensor principal axis and the c-axis of the crystal.

φ is the angle between the projection of the tensor principal axis on (ab)-plane and a-axis.

In general this group consists of two central lines and each central line is flanked by two satellites which can be interpreted due to tungsten W^{183} hyperfine interaction. Along crystal c-axis the two sets of lines merge into one set with $g = 1.80$. The principal values of the g-tensors and the directions of the axes were found and shown in Table II.

The hyperfine separation is 51 gauss along the crystal c-axis, and varies from 54 to 120 gauss in the (001) plane. The maximum and minimum separations occur at one degree off [110] as shown in Figure 17. The directions of g_x and g_y are approximately parallel to the directions of a tungsten atom and its nearest metal neighbors (calcium atoms) in the crystal. The crystal structure of calcium tungstate indicates that there are four nearest calcium atoms to each tungsten atom. If the beta spectrum is due to paramagnetic tungsten with one of its four calcium neighbors being displaced, in general there should be four sets

of lines due to four possible orientations of the paramagnetic defects. However, due to the fact that the four nearest calcium atoms form a square planar configuration with the tungsten atom situated at the center, the four different orientations of the defects become two equivalent pairs so far as the applied magnetic field is concerned. This is evidenced by the fact that experimentally only two sets of beta lines are observed. It is therefore concluded that the beta center is due to paramagnetic tungsten with one of the nearest calcium neighbors displaced. The beta center is not as stable as the gamma center. Four weeks after irradiation the intensity is reduced approximately by half. It can also completely be annealed out by heating up to 600°C for about an hour.

Since very little work has been done on ESR of $5d^1$ configuration, the study of W^{5+} has interest of itself. There have been two tungsten centers reported in $CaWO_4$. Zeldes[58] reported a center produced by irradiating calcium tungstate single crystals with gamma rays at 77°K and indicated that it could be WO_4^{---} near a lattice defect. The hyperfine interaction of Zeldes' center varies from 35 to 65 gauss and the principal axis directions and principal values of g-tensors are as follows:

	Direction Cosines			g
	a	b	c	
g_1	.574 (56°48')	-.837 (146°53')	.008 (89°31')	1.5716
g_2	.832 (32°39')	.543 (57° 5')	-.111 (96°24')	1.6334
g_3	.089 (84°52')	.068 (86° 4')	.994 (5°)	1.8482

Azarbayejani[60] reported a W^{5+} center in vacuum reduced $CaWO_4$:Y . The parameters at $\theta = 90°$ ($H \perp c$) are $g_1 = 1.587$, $g_2 = 1.600$ $A_1 = 53.3$, $A_2 = 66.35$ G, and at $\theta = 0°$($H // C$) are $g = 1.850$ and $A = 19.05$ G .

It is interesting to notice that the reported parameters for Zeldes' and Azarbayejani's centers are very close to each other. It strongly suggests that both are WO_4^{---} centers associated with a lattice defect. The parameters of the beta center also fall close in this category and the orientation of the g-tensor further indicates that the associated defect is the nearest calcium displacement. The unusually large hyperfine interaction of the gamma center indicates that it is of quite different structure from the other tungsten centers, namely, one of the oxygens of the tungstate itself being displaced.

3.2 Uniaxially Stressed Electron Spin Resonance

From the simple electron spin resonance result it is conclude that the beta centers and the gamma centers are due to paramagnetic tungstens associated with calcium and oxygen vacancies respectively. In order to obtain further information about these centers, some dynamical methods have to be employed and to obtain further information by observing the response of the ESR spectrum. The application of uniaxial stress can destroy the equivalence of different defect sites along specified directions. As the gamma centers are due to tungstates with oxygen vacancies, the four tungsten-oxygen bond directions provide four different sites for defect centers. As uniaxial stress is applied the potential energy of one site may increase more than other sites. If the defects are allowed to reorient themselves, the site with higher energy will be

expected to be less populated and vice versa. This will manifest itself by the change in the relative intensities of ESR lines. With the stress used here the effect of linewidth dependence upon orientations due to stress is assumed to be small and only the heights of the lines are measured.

Uniaxial stress experiments have been carried out with a maximum stress of 11,000 psi along the [110] direction of the crystal. In this case two of the four sites, namely γ_1 and γ_2 will make an angle of 36° with the applied stress by γ_3 and γ_4 will make equal angles of 79° with the stress. Thus it is expected that the effect of uniaxial stress is to change the intensities of γ_1 and γ_2 in the same way and change γ_3 and γ_4 in the same way. Since the total number of defects is not changed by the stress, the gaining in intensity of one group must be conpensated by intensity reduction of the rest. This has been confirmed experimentally. The following table indicates the change in intensities of gamma-lines with and without stress

	γ_1	γ_2	γ_3	γ_4
11,000 psi	58	65	58	59
0 psi	49	62	63	65
change in intensity	$\Delta\gamma_1 + \Delta\gamma_2 = 12$		$\Delta\gamma_3 + \Delta\gamma_4 = -11$	

No such effect is expected for the beta lines. From the crystal structure each calcium atom is equivalently associated with four closest tungsten neighbors. In other words, the beta centers are built by pairs of differently oriented defects. Uniaxial stress cannot lift the orientation degeneracy or induce population difference. Experimentally, no

measurable change in relative intensities of the beta lines is observed in agreement with the prediction. Therefore it is concluded that the uniaxial stress experiment provides further support for the previous assignment of beta and gamma centers.

3.3 The Number of Gamma Centers

The difficulties encountered in measuring spin concentrations and the relative merits of several approaches to the problem are discussed in References 61 through 69. The methods used here is similar to that of Singer and Kommander.[69] Under proper conditions the static spin susceptibility χ_0 is related to P , the power absorbed in an electron spin resonance experiment at magnetic field H , by the expression

$$\chi_0 = \frac{4\gamma}{\pi \omega^2 H_1^2} \int_0^\infty P\, dH \qquad 3.3-1$$

Where $\gamma = g\beta/\hbar$ is the gyromagnetic ratio, and ω is the angular frequency of the rf field which has an amplitude H_1 inside the sample. This relationship will hold only if the following conditions are met: (1) the spin system must be in thermal equilibrium with its surroundings; i.e. saturation must be absent. (2) The linewidth must be small compared to the magnetic field at resonance. (3) The modulation amplitude must be small compared to the line-width. (4) Skin effects must be absent.

The absence of saturation was evidenced by examining the signal height as a function of incident power. Examination of the linewidth of the gamma centers showed that the second condition was met. Modulation amplitude was minimal ($<.5$ G). Symmetry of the signals showed skin effect to be absent.

In practice, reference samples of known spin concentration were used so that the spin susceptibilities and concentrations could be obtained from the expression

$$\frac{n}{n^*} = \frac{\chi}{\chi^*} = K\left(\frac{g}{g^*}\ \frac{h}{h^*}\ \frac{A}{A^*}\ \frac{H_m}{H_m^*}\right)\left(\frac{\Delta H}{\Delta H}\right)^* \qquad 3.3\text{-}2$$

where n is the concentration or number of spins,

g is the spectroscopic splitting factor,

χ is the susceptibility

h is the signal height,

A is the amplitude gain,

H_m is the modulation amplitude,

ΔH is the line width and

K is a factor depending on the line shapes of the reference and the sample.

The starred values and unstarred values pertaining to the reference and the sample respectively.

Equating n/n^* to χ/χ^* assumes that both systems would obey Curies law at fixed spin concentrations. Measurements of K , which related the line shape of the reference to that of the unknown sample, is required for the evaluation of spin concentrations. To accomplish this, line shape analysis was applied to both the reference and the sample.

The method of line shape analysis used was similar to that used by Weidner and Whitmer[70] for an absorption curve. If one measures the widths of an experimental derivative curve at various fractional heights and plots these widths against the width at the same fractional

heights for some theoretical derivative curve, a straight line result will indicate the experimental and the theoretical curves to have the same shape.

The reference sample used was $CuSO_4 \cdot 5H_2O$ in single crystal form. It has very small Weiss constant so that Equation (3.3-2) is applicable. Single crystals of convenient size (a few hundred micrograms) can be chosen directly from a reagent bottle of the chemical, weighed on an electro-balance and then imbedded in paraffin. The standard sample was simply glued to the side of the calcium tungstate crystal during measurement. It has been reported that no change in the ESR properties was observed over a period of several years. The line width and the g-values are both orientation dependent. The line shape has been reported to be Lorentzian.(62-65)

Figure 19 is the first derivative absorption curve of the gamma-centers. The line shape analysis is shown in Figure 20. Neither the plot against Gaussian nor against Lorentzian gives a straight line. The downward curvature of the lower curve implies that a Lorentzian curve gets broader in the wings faster than the experimental resonance curve of the gamma centers. The upward curvature of the upper curve implies that a Gaussian curve gets narrower in the wings faster than the gamma lines. The experimental curve is intermediate between Gaussian and Lorentzian. A straight line can be obtained if the line shape is assumed consisting of 65 percent Gaussian and 35 percent Lorentzian. Since the standard sample is of Lorentzian shape, the constant K in Equation (3.3-2) is equal to unity if the unknown is also of Lorentzian shape and $K = .29$ if the unknown is of Gaussian shape.(69) For the case of gamma center, we have $K = .65 \times 1 + 0.29 \times .35 = 0.75$.

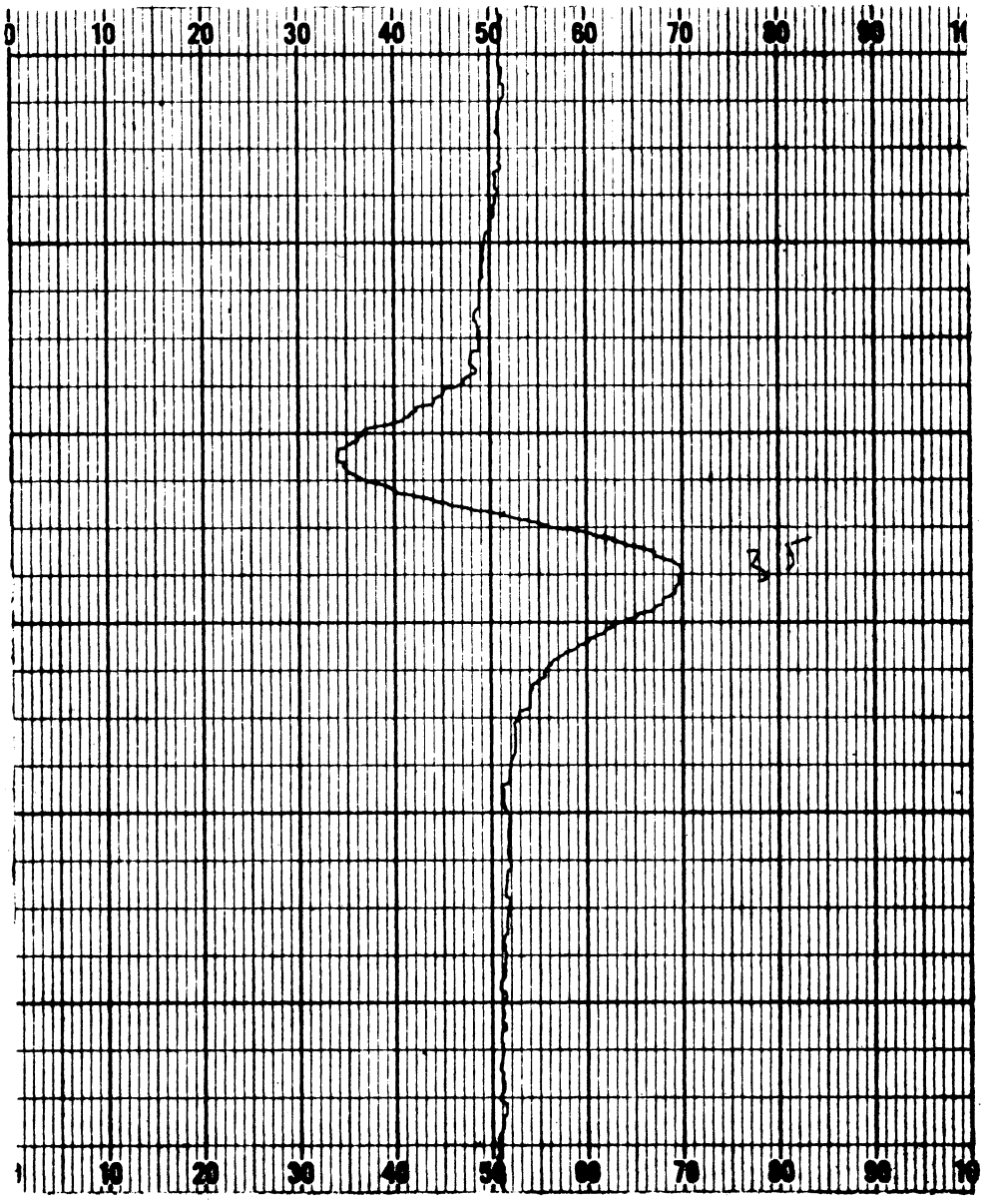

Figure 19. Line Shape of the γ-center.

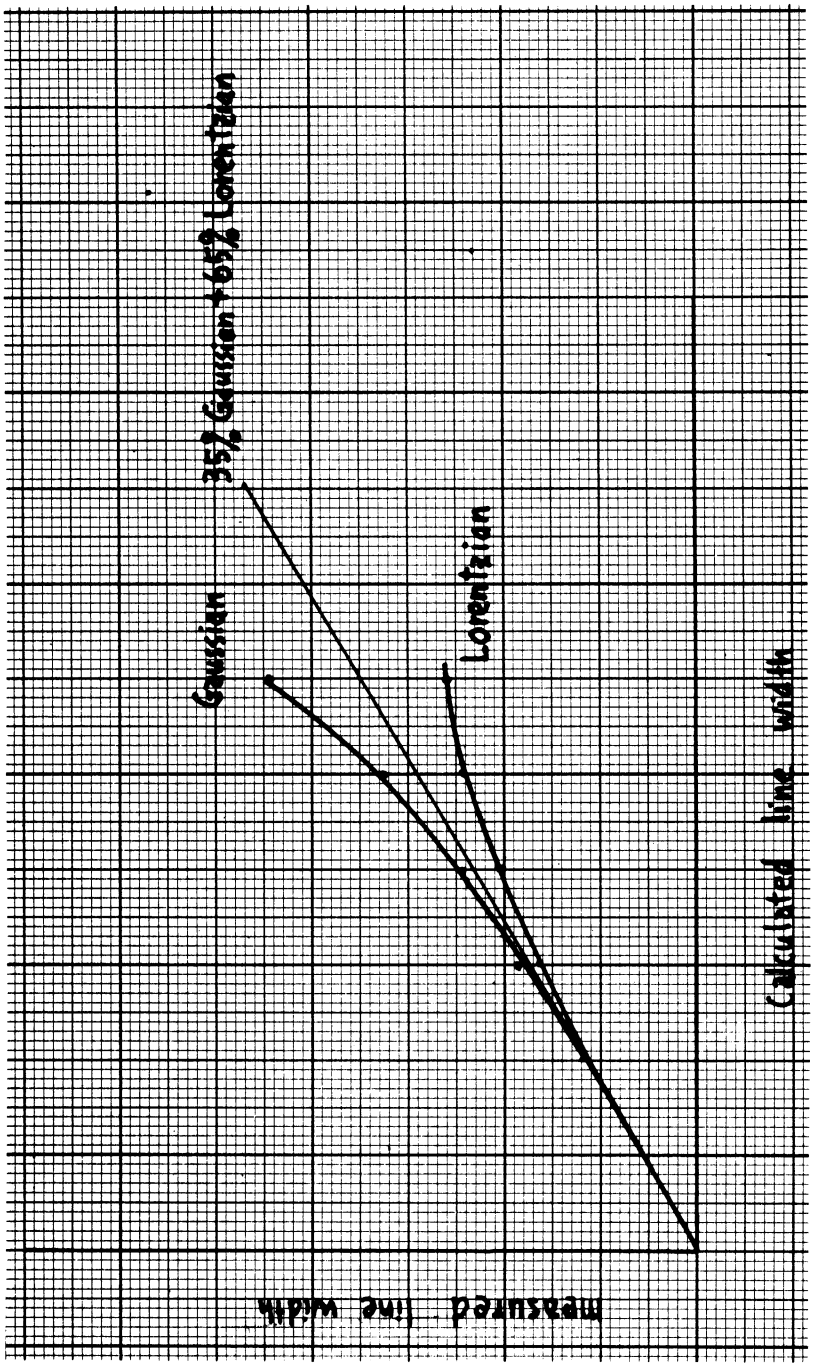

Figure 20. Line Shape Analysis for the γ-center.

Experimentally, using a copper sulfate standard of 1.52 milligrams attached to the surface of the calcium tungstate crystal, the amplitude gain will be the same, i.e. $A = A^*$ and the modulation will be the same too, i.e. $H_m = H_m^*$. The g-values and the line widths and the signal heights are measured as follows:

$$g_{Cu} = 2.15$$

$$g_\gamma = 1.66$$

$$[h(\Delta H)^2]_{Cu} = 4262$$

$$[h(\Delta H)^2]_\gamma = .648$$

The number of spins in the standard was

$$n_{Cu} = 3.66 \times 10^{18}$$

The constant K is given by

$$K = 0.75$$

Using the relation

$$\frac{n_\gamma}{n_{Cu}} = K \left(\frac{g_\gamma}{g_{Cu}} \frac{h_\gamma}{h_{Cu}} \frac{A_\gamma}{A_{Cu}} \frac{H_m^{Cu}}{H_m^\gamma} \right) \left(\frac{\Delta H_\gamma}{\Delta H_{Cu}} \right)^2 \qquad 3.3-3$$

the total number of gamma centers of the calcium tungsten single crystal of 270 milligrams after one hour of reactor neutron irradiation was found to be

$$n_\gamma = 1.29 \times 10^{16} \quad \text{spins}$$

The calculation of the number of displacement is divided into two parts according to the neutron flux distribution. Above 0.5 Mev where fast neutron flux was measured, numerical integration gave the number of displacements. Below 0.5 Mev where 1/E neutron flux is assumed, number of displacements is obtained by direct integration. Data used during calculation are as follows:

average neutron cross section from BNL-325

$$\sigma(O) = 3 \times 10^{-24} \quad cm^2$$

$$\sigma(Ca) = 3 \times 10^{-24} \quad cm^2$$

$$\sigma(W) = 10 \times 10^{-24} \quad cm^2$$

ionization potential from § 1.4

$$E_L = 4.95 \text{ ev}$$

displacement energy

$$E_d = 25 \text{ ev}$$

weight of calcium tungstate sample

$$W = 270 \text{ mg}$$

irradiation time

$$T = 3600 \text{ sec.}$$

correction factor for anistropy and inelasticity of collision from Dienes and Vineyard[41]

$$f = 0.67$$

Total number of displacements due to fast neutron flux with E > 0.5 Mev: Within this region the primary recoil energy is smaller than the limiting ionization energy for tungsten but is larger than the limiting ionization energy for both oxygen and calcium. For tungsten as primary the number of displacements was calculated from the following:

E (Mev)	neutron flux	E/A	E/A · Φ
1	2.8 x 10^{11} / cm^2-s-Mev	5465	1.56 x 10^{15}
2	2.7 "	10929	2.983 "
3	2.2 "	16393	3.623 "
4	1.2 "	21858	2.601
5	.88 "	27322	2.404 "
6	.46 "	32787	1.508 "
7	.25 "	38251	.956 "
8	.13 "	43516	.568 "
9	.07 "	49180	.344 "
10	.03 "	54650	.164 "

$$\Sigma \frac{E}{A} \Phi = 1.67 \times 10^{16}$$

For tungsten as primary the number of displacements due to fast neutron with E > 0.5 Mev is given by

$$N_w = 1.38 \times 10^{16} \text{ displacements}$$

For both oxygen and calcium as primaries the total number of displacements was as follows:

$$N_{Ca} + N_O = 1.56 \times 10^{16} \text{ displacements}$$

Total number of displacements due to epithermal neutron flux ($E < 0.5$ Mev):

The average energy trasnfer for a 1/E flux is given by

$$\bar{E} = \frac{E_p}{2} \Big/ \ln\left(\frac{E_p}{E_d}\right)$$

Below 0.5 Mev, E was less than E_t, the limiting ionization energy for oxygen calcium and tungsten as primaries.

	$E_p = 4E/A$	E/E	$\ln E/E$	$\bar{E}$	Φ	$\Phi \cdot \bar{E} \cdot \sigma$
O	125000	5000	8.51	7349	1.74×10^{12}	15.38×10^{-8}
Ca	50000	2000	7.59	3794	1.46×10	1.44×10
W	10929	437	6.08	899	1.23×10	1.11×10

$$\therefore N_{\gamma_E} = .72 \times 10^{16} \text{ displacements}$$

After introducing the correction factor for anisotropy and inelasiticity in fast neutron scattering, the total number of gamma centers was found as follows:

$$N_\gamma = \frac{2}{3} \cdot \frac{2}{3} \left(N_{Ca} + N_O + N_W + N_{\gamma_E} \right)$$

$$= 1.63 \times 10^{16} \text{ displacements}$$

4. RESULTS AND DISCUSSIONS-PARAMAGNETIC NIOBIUM (71)

4.1 Importance and Motivation

Single crystals of calcium tungstate doped with trivalent Nd^{3+} ions have been used extensively for solid state lasers.(1,2) Although rare-earth ions can be introduced into calcium tungstate without a secondary charge compensating ion (creating a defect lattice), charge compensation by a second ion is generally preferred since it simplifies the fluorescent emission spectrum and ESR spectrum as well as lowering the threshold for laser action of the crystals.(16-18)

The trivalent Nd^{3+} ions are believed substitutionally located at calcium sites in the calcium tungstate crystals. Pentavalent Nb^{5+} ions located substitutionally at tungsten sites will be an ideal charge compensator by the following relation:

$$(Nb^{5+} + Nd^{3+}) \text{ substitute for } (W^{6+} + Ca^{2+})$$

The study of ESR of niobium undoubtedly will provide information about the problem of charge compensation. Furthermore the study of Nb^{4+} itself is of importance since it provides information of the comparatively little studied $4d^1$ electron configuration.

In the periodic table niobium is the element just below vanadium. Radiation chemistry of vanadium in solids has been one of the active research programs in our Laboratory. In particular, the study of vanadium in calcium tungstate as a charge compensator has just been completed.(72) Our present work on $CaWO_4$:Nb is just the starting of the study program of niobium and can also be considered as a further extension of the vanadium program.

The ESR results of $CaWO_4$:Nb are summarized as follows:

Before irradiation, niobium in tungsten site is the diamagnetic Nb^{5+}. After irradiation, it acquires one electron and becomes paramagnetic Nb^{4+}. At 195°K the niobium ESR spectrum is of slightly axial symmetry with

$g_{\parallel} = 2.023$

$g_{\perp} = 2.026$

$A = 29$ gauss

$B = 29.2$ gauss

where the symmetry axis is along the crystal c-axis. As temperature decreases, the spectrum is broadened at first and finally splits into four at 77°K. The average position of the low temperature spectrum is equal to the position of the high temperature spectrum. This interesting problem of temperature dependence is explained in terms of vibronic interaction.

4.2 Properties of Niobium and Vanadium

As a comparison and reference we list the pertinent properties of niobium and vanadium as follows:

	Nb	V
Atomic Number	41	23
Isotope Abundance	100%$Nb^{(93)}$	100%$V^{(51)}$
Nuclear Spin	9/2	7/2
Nuclear Moment	6.1435	5.1392
Nuclear g-value	1.37	1.47
Electron Configuration	[Kr]4d'	[Ar]3d'

Gamma or X-radiation can change the valence state of Nb and V as follows:

$$V^{5+} \xrightarrow{X,\ r} V^{4+}$$

$$Nb^{5+} \xrightarrow{X,\ r} Nb^{4+}$$

The only difference is that for V the valence change occurs at room temperature but for Nb lower temperature (liquid nitrogen temperature) is needed.

4.3 Results of ESR Measurements

ESR absorption of niobium doped calcium tungstate single crystals were studied at microwave frequency of 16.5 Gc/sec (Ku-band). Three samples were studied.

a, $CaWO_4$: .5% Nb

b, $CaWO_4$: 1% Nb 1% Na

c, $CaWO_4$: 1% Nb 1% U

No ESR signal is detected at room temperature and liquid nitrogen temperature before irradiation. After Co^{60}-gamma irradiation of about 10^6 rads, groups of lines are observed at 195°K and 77°K.

a. Dry Ice Temperature (195°K)

At dry ice temperature, the spectrum always consists of two lines with axial symmetry. It can be described by the spin Hamiltonian

$$\mathcal{H} = \beta \left[g_{\parallel} H_z S_z + g_{\perp} (H_x S_x + H_y S_y) \right] + A_z I_z S_z + B (I_x S_x + I_y S_y)$$

with $S = 1/2$ and $I = 9/2$. The measured constants are

$g = 2.023$

$g = 2.026$

$A = 29$ gauss

$B = 29.2$ gauss

where the symmetry axis is along the crystal c-axis.

b. Liquid Nitrogen Temperature (77°K)

At liquid nitrogen temperature each line in general splits into four. The four sets of ten lines coalesce into one when the magnetic field is along the c-axis and this is shown in Figure 21. In the (ab) plane only two sets of ten lines are observed. Figure 22 is the ESR spectrum when the magnetic field is along [110] direction. The average position of the sets of lines is equal to the position of the single set of 195°K. Figure 23 shows the line positions when the magnetic field is varied in the (ab) plane. For the reason of clarity only the angular variation of the g-values has been plotted. The two sets of g-values become identical when the magnetic field is 17° from the a-axis in the (ab) plane.

c. Niobium Site

The ESR spectrum consists, essentially, of sets of ten lines of almost equal intensities and separation, thus suggesting a hyperfine structure with nuclear spin $I = 9/2$ and 100 percent natural abundance. Besides niobium, bismuth (Bi-209) is the only isotope with nuclear spin $I = 9/2$ and 100 percent natural abundance. Since niobium is the intentional dopant the observed ESR lines are attributed to niobium.

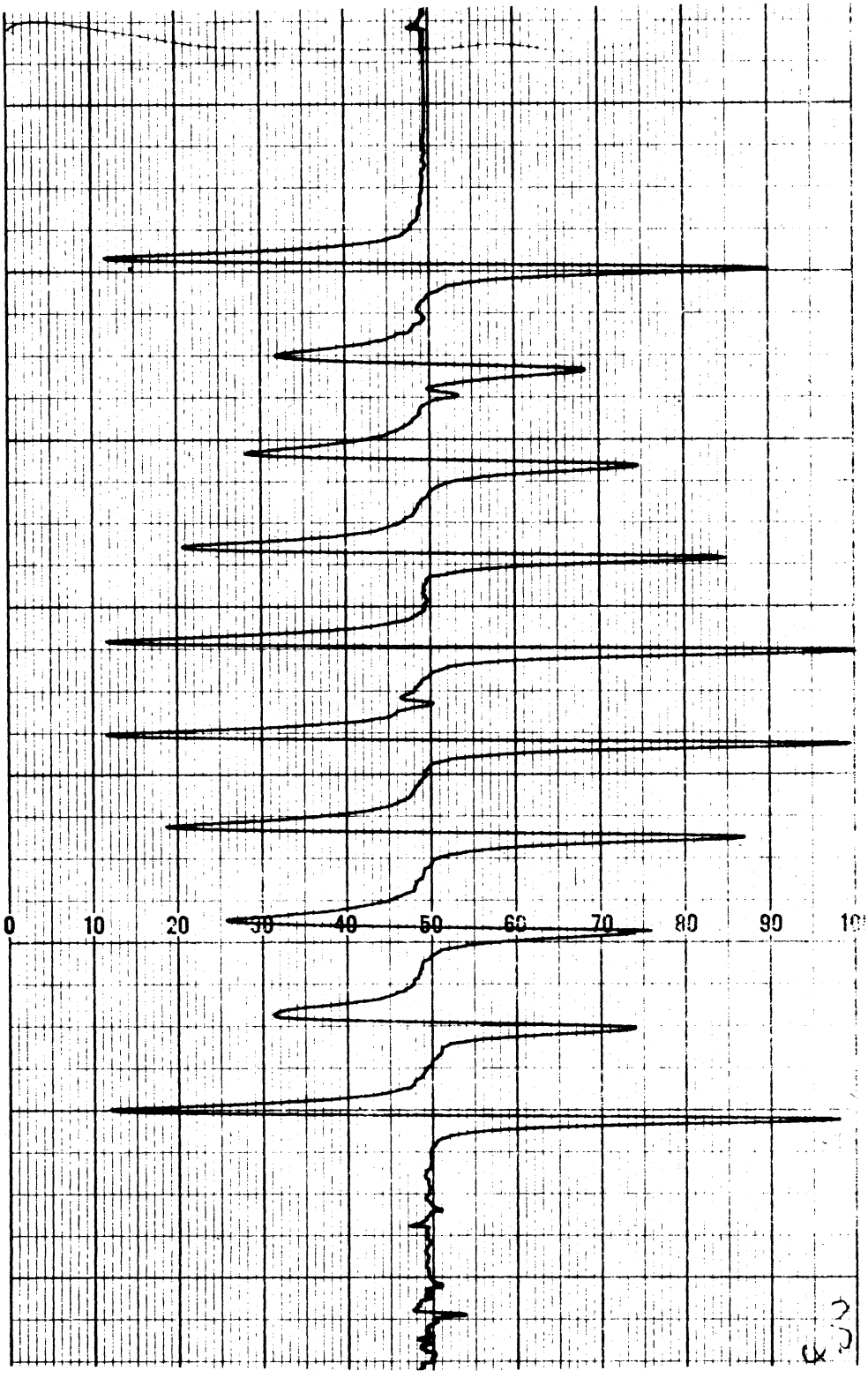

Figure 21. ESR Spectrum of $CaWO_4$: Nb^{4+} at 77°K, H Parallel to the [001] Axis.

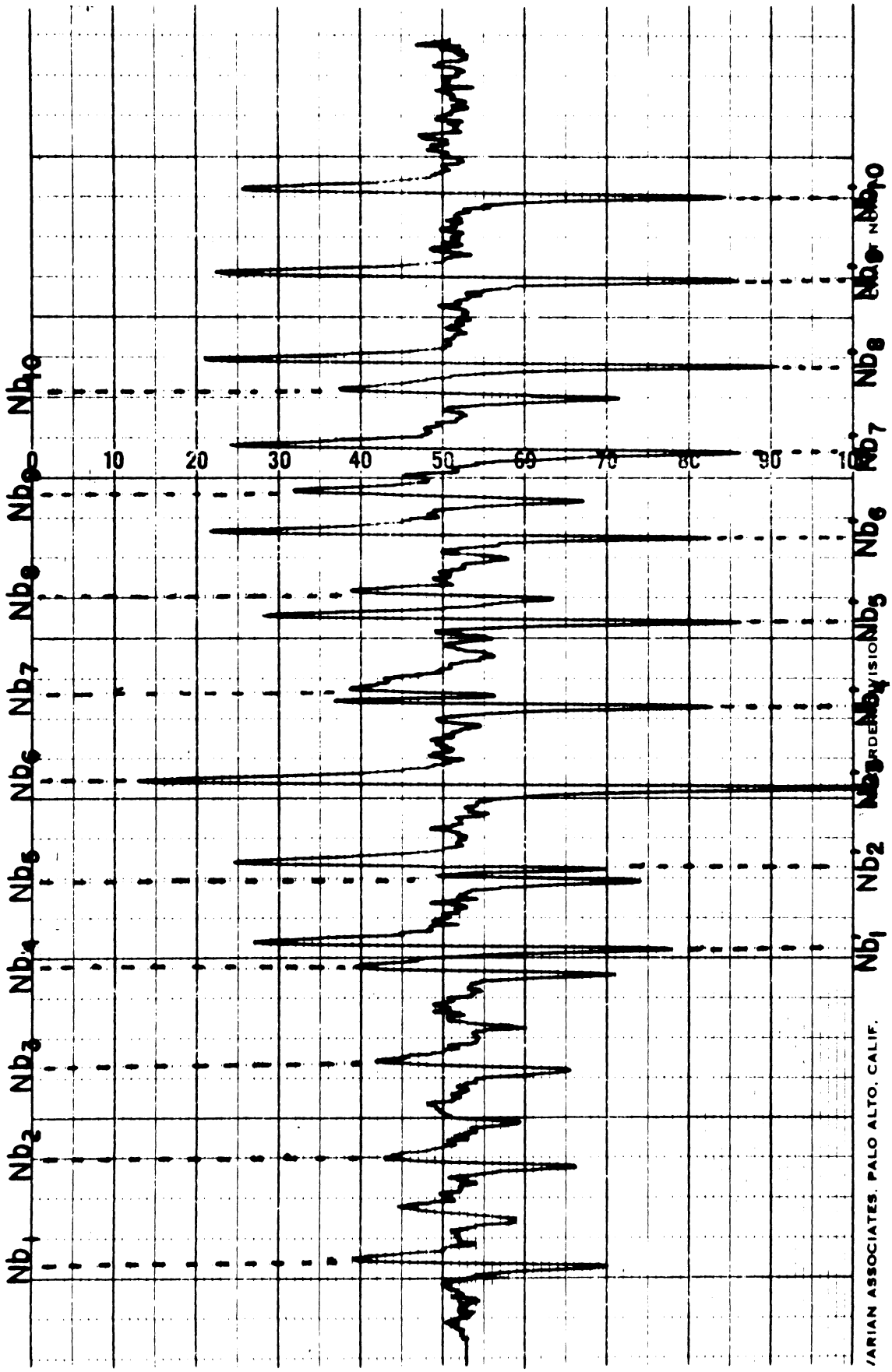

Figure 22. ESR Spectrum of $CaWO_4$: Nb^{4+} at 77°K, H Parallel to the [110] Axis.

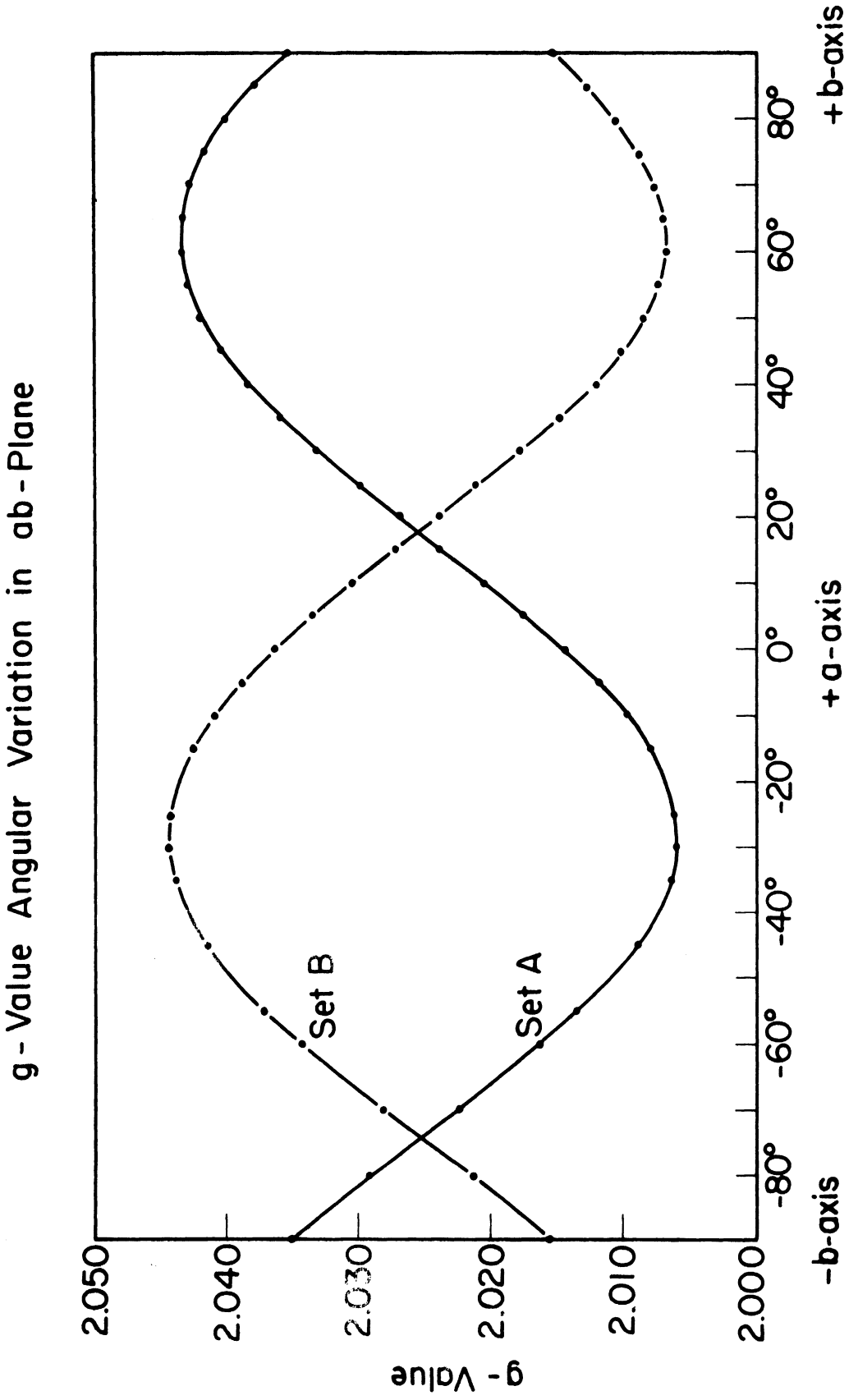

Figure 23. g-value Angular Variation of $CaWO_4$: Nb at 77°K, H in the (ab)-plane.

The ESR results of niobium can be explained by the model that niobium occupies the tungsten site substitutionally as has been inferred from chemical evidence. Before irradiation, niobium in tungsten site is the diamagnetic Nb^{5+} . After irradiation, it acquires one electron and becomes the paramagnetic Nb^{4+} ion.

The symmetry of the Nb spectrum does not rule out the possibility of the Nb^{4+} at a Ca-site. That Nb^{4+} is assigned to a covalent W-site rather than at a ionic Ca-site is evidenced by the following arguments:

1. Radii: The radii of Nb, Ca and W are 1.342, 1.736 and 1.304 Å respectively. Nb size is much closer to W than Ca.

2. Valencies: The valencies of Nb, Ca, and W are +5 , +2 and +6 respectively. From charge consideration Nb is more likely to substitute for W .

Convincing evidence that Nb is in the covalent W-site rather than the ionic Ca-site can be obtained when we examine the published ESR data on Nb . Vinokurov et al.[73] reported Nb in zircon. Chester[74] reported Nb in rutile and Rasmussen[75] reported ESR of pentachloromethoxoniobate $Nb(OCH_3)Cl_5^{2-}$. These results are shown as follows:

Samples	Δg	Hyperfine Interaction
Zircon: Nb	$\Delta g_{\parallel} = -.151$, $\Delta g_{\perp} = -.115$	A = 309G , B = 138G
Rutile: Nb	$\Delta g \simeq .035$	$\langle A \rangle$ = 90 gauss
Nb(OCH)Cl	$\Delta g_{\parallel} = -.058$, $\Delta g_{\perp} = -.114$	A = 248G , B = 144G

In all these cases Nb is located in an ionic site. Notice that the reported Δg's are all negative and the hyperfine interactions are large. Now in calcium tungstate things are different.

3. Hyperfine Interaction: The Nb hyperfine interaction in calcium tungstate is about 29G. which is much smaller than the reported values. This is taken as a strong evidence that Nb is in a covalent W-site.

4. g-values: The observed Δg's for Nb in $CaWO_4$ are all positive in contrast to the reported values in ionic sites. This is evidenced as Nb is in the covalent W-site, and the arguments are as follows:

Δg is given by (see appendix)

$$\Delta g_j = -\frac{\lambda}{E - E_0} |\langle \psi_i | L_j | \psi_i \rangle|$$

where the spin orbital coupling constant λ is positive for our case of Nb^{4+}. In an ionic site, crystal field splitting is a good approximation. All levels contributing to Δg's have energies higher than the ground state, i.e. $E > E_0$. Thus Δg's are all negative as reported. In the case of a covalent site, we have to consider the molecular orbital scheme.[76] In this case we need to consider the filled levels with paired spins below the ground level as well as the empty levels above the ground. The positive g-shift is due to the fact that we can excite one of the paired spins into an originally unpaired state. This transition affects electrons with opposite spin and can make Δg positive.

4.4 Temperature Dependence--Main Problem

It is interesting to observe the temperature dependence of the spectrum. At 77°K, if the magnetic field is in arbitrary direction, in general the spectrum consists of four sets of ten lines around the position with $g = 2$. As the temperature increases, the lines are broadened at first then collapse. Finally, at 195°K one set of ten lines emerges at the average position of the four sets of 77°K.

Figure 24 shows the spectrum change when the temperature is varied from 77°K to 195°K. Since the magnetic field is along the [110] direction, there are only two sets of ten lines instead of four at 77°K as shown in Figure 24a. As the temperature increases to about 100°K, the lines are broadened as shown in Figure 24b. As the temperature increases further to about 150°K, the niobium spectrum disappears. The lines shown in Figure 24c are due to Mn^{++} and the quartz holder. Finally at 195°K one set of lines emerges at the average position of the two sets at 77°K as shown in Figure 24d.

The temperature dependence of the spectrum can be explained in terms of vibronic interaction and will be discussed in detail in the sections to follow.

4.5 Proposed Model

The proposed model to explain the experimental results is as follows:

Without vibronic interaction, the Nb is located at the center of the NbO_4 bisphenoid with D_{2d} symmetry. Considering vibronic interaction, the Nb atom will displace in the x-y plane ((a,b) plane of the crystal) and can have four energy traps along the four oxygen projections in the x-y plane.

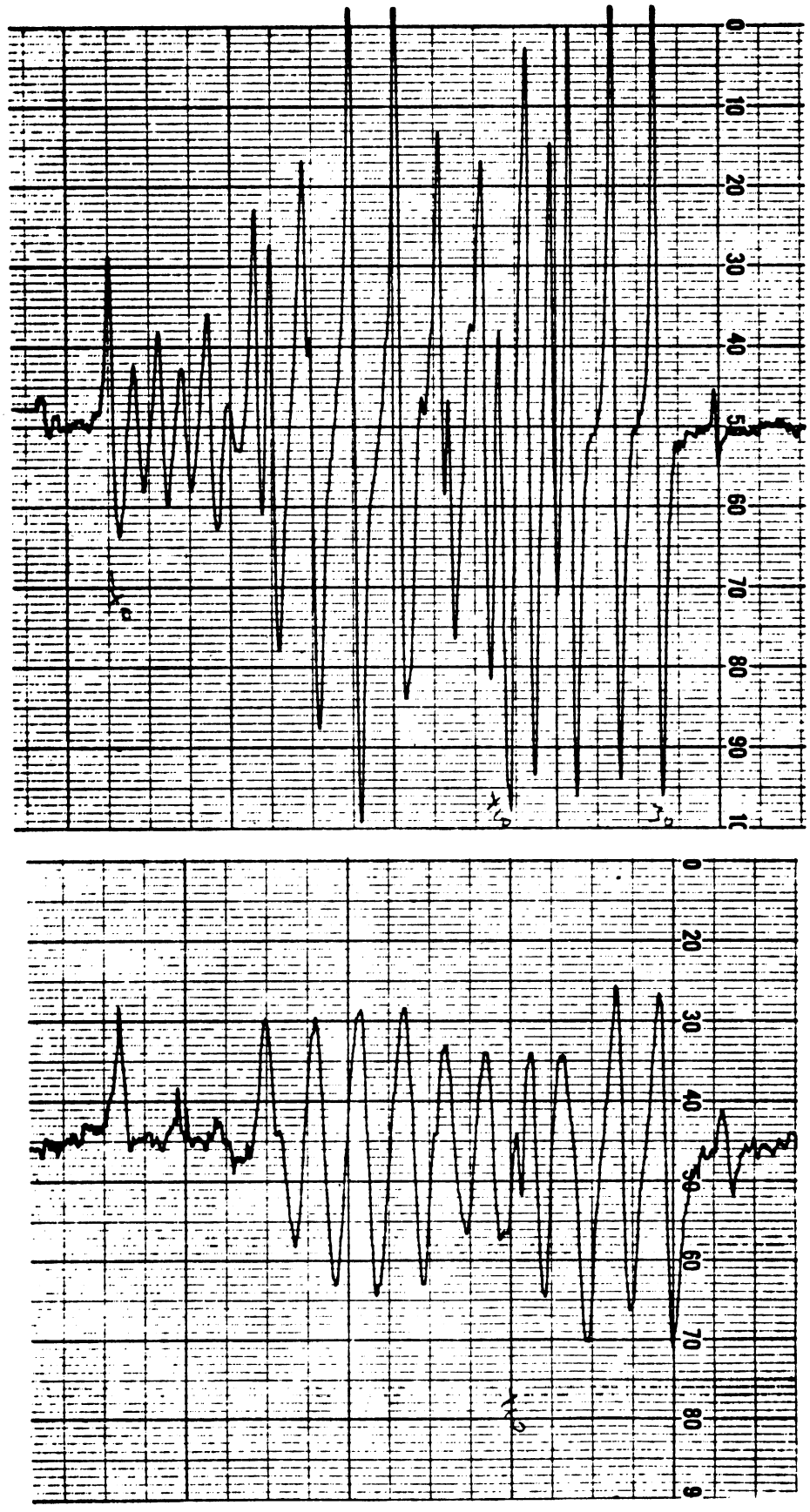

Figure 24. Temperature Dependence of Nb^{4+} Spectrum.

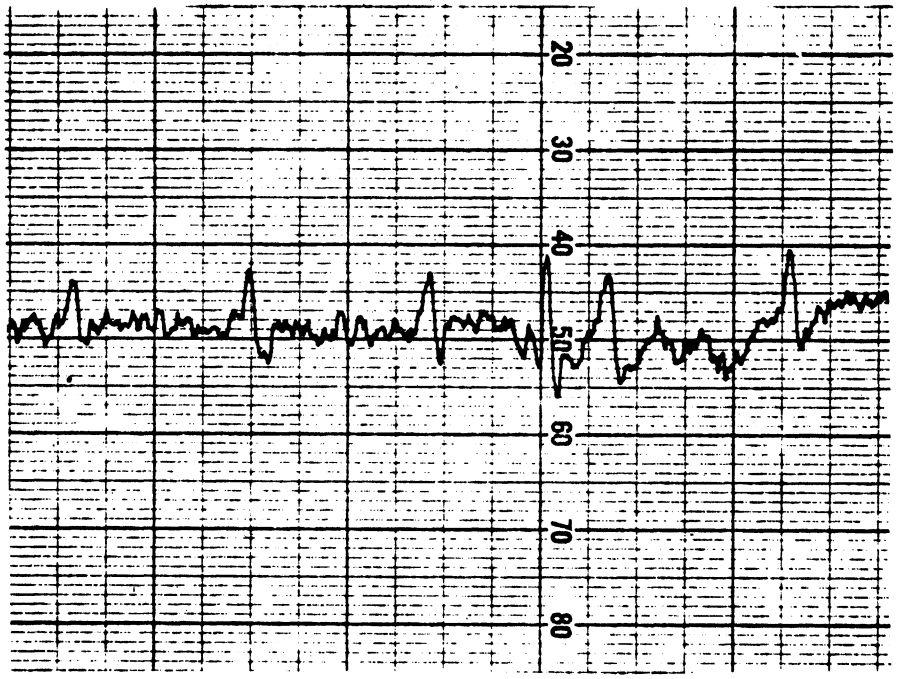

c

150°K

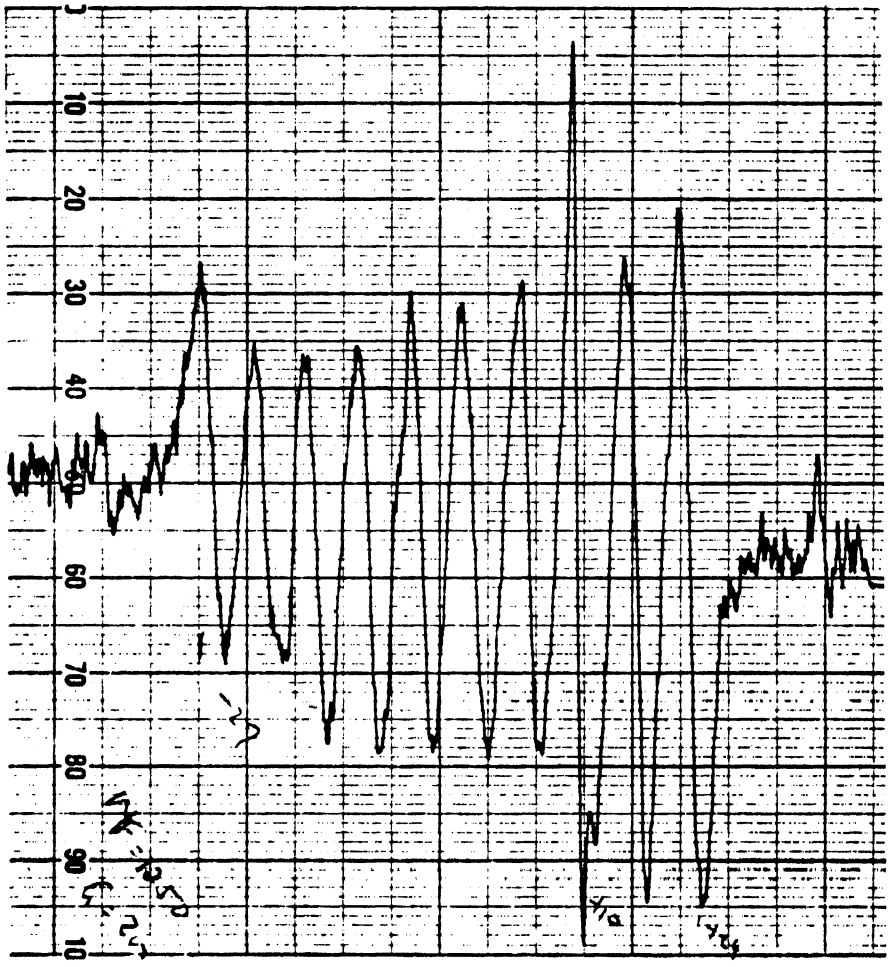

d

195°K

Figure 24. Continued.

We shall start by constructing the Hamiltonian. Using the unperturbed NbO_4 bisphenoid with D_{2d} symmetry as the zero-th order approximation and considering linear and quadratic nuclear displacments only, the perturbation matrix is set up and simplified by symmetry arguments. After extremization of the energy with respect to the nuclear coordinates it can be shown there are indeed four energy traps which account for the splitting of the ESR spectrum. The assumptions and arguments leading to the above mentioned results are given in detail in the following sections.

4.6 Normal Vibrations of NbO_4

Since we shall try to explain the experimental results in terms of vibronic interaction and it is much simpler to use the normal displacements classified according to the irreducible representations of the symmetry group than the nuclear coordinates directly, we shall first briefly discuss the normal vibrations.

The nine normal displacements of a $D_{2d}(NbO_4)$ molecule are shown in Figure 25. Their symmetries are as follows:

Normal modes	q_1	q_{2a}	q_{2b}	q_{3a}	q_{3b}	q_{3c}	q_{4a}	q_{4b}	q_{4c}
Symmetry	A_1	A_1	B_1	B_2	E	E	B_2	E	E

As shown in Figure 25, q_1 is the totally symmetric vibration, q_{2a} and q_{2b} are the torsion vibrations, q_{4a} q_{4b} and q_{4c} are distortion vibrations. q_{3a} q_{3b} and q_{3c} are displacement vibrations. For the q_1, q_{2a}, q_{2b}, q_{4a}, q_{4b} and q_{4c} vibrations the central Nb atom is stationary, while the displacement vibrations arise from the motion of the four oxygens as a whole relative to the niobium atom. According

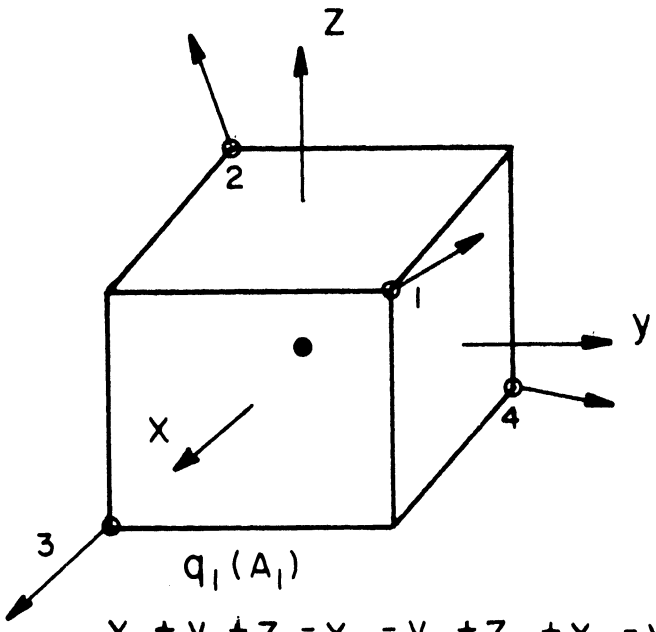

$q_1(A_1)$

$X_1 + y_1 + Z_1 - X_2 - y_2 + Z_2 + X_3 - y_3 - Z_3 - X_4 + y_4 - Z_4$

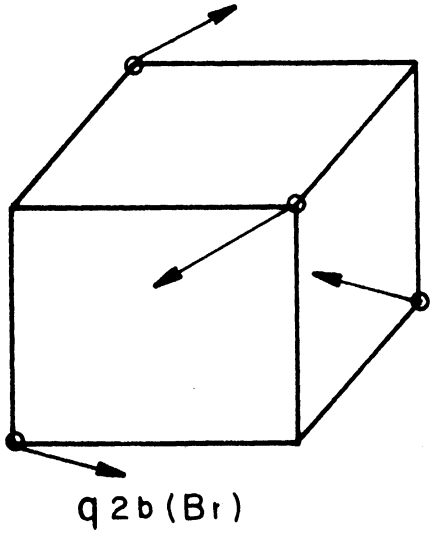

$q_{2b}(B_1)$

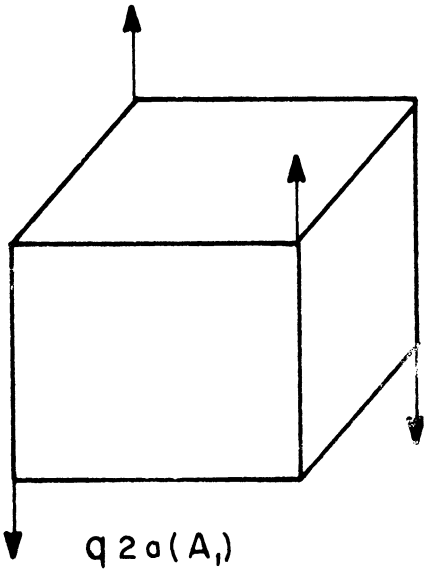

$q_{2a}(A_1)$

$X_1 - y_1 - X_2 + y_2 + X_3 + y_3 - X_4 - y_4$ $\qquad$ $Z_1 + Z_2 - Z_3 - Z_4$

NORMAL VIBRATIONS of a D2d XY4 MOLECULE

Figure 25. Normal Vibrations of a D_{2d} XY_4 Molecule.

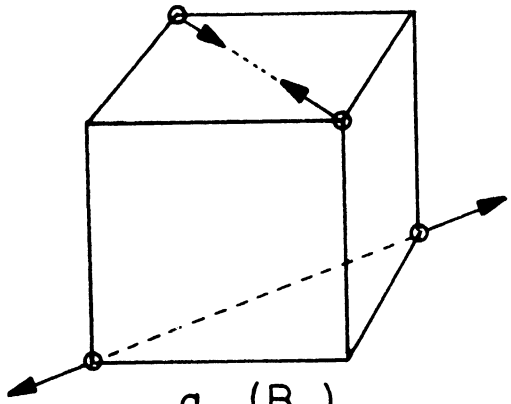

$q_{4a}(B_2)$

$-x_1-y_1+x_2+y_2+x_3-y_3-x_4+y_4$

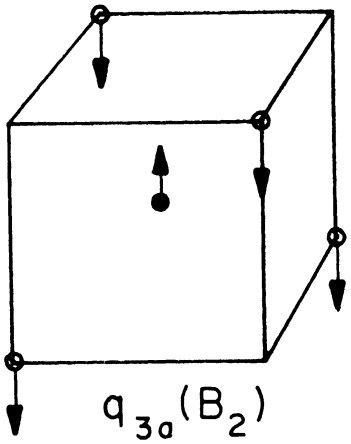

$q_{3a}(B_2)$

$\alpha z_0-\beta(z_1+z_2+z_3+z_4)$

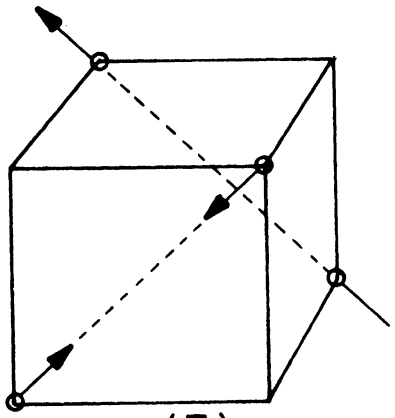

$q_{4b}(E)$

$-y_1-z_1-y_2+z_2+y_3+z_3+y_4-z_4$

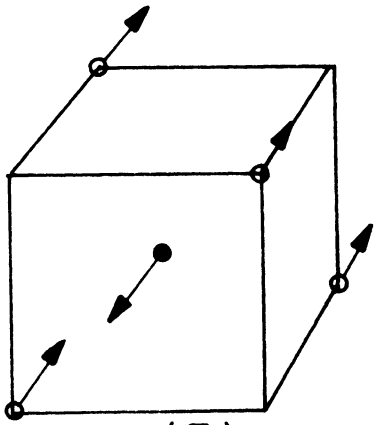

$q_{3b}(E)$

$\alpha x_0-\beta(x_1+x_2+x_3+x_4)$

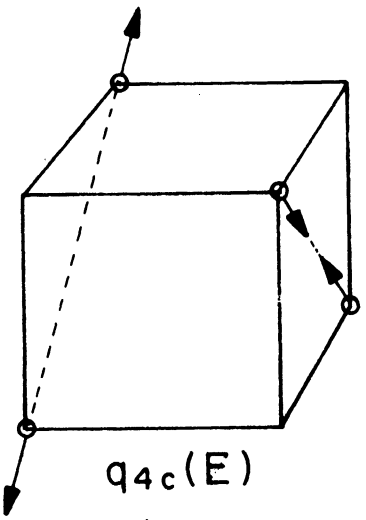

$q_{4c}(E)$

$-z_1-x_1+z_2-x_2-z_3+x_3+z_4+x_4$

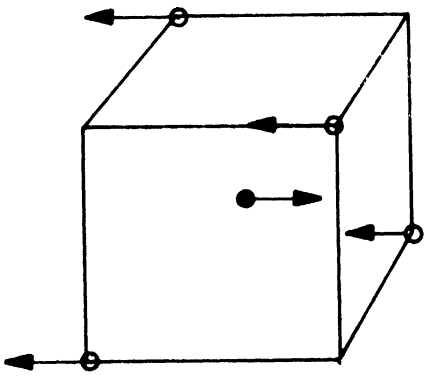

$q_{3c}(E)$

$\alpha y_0-\beta(y_1+y_2+y_3+y_4)$

Figure 25. (Continued)

to our proposed model the central Nb will be distorted in the x-y plane, hence the only normal vibrations we shall be concerned with are the q_{3b} and q_{3c} . The transformation property of linear and quadratic terms of q_{3c} and q_{3c} as well as the character table for D_{2d} group are shown in Table III, namely

$$q_{3b},\ q_{3c} \quad : \quad E$$

$$q_{3b}^2 + q_{3c}^2 \quad : \quad A_1$$

$$q_{3b}^2 - q_{3c}^2 \quad : \quad B_1$$

$$q_{3b}\ q_{3c} \quad : \quad B_2$$

TABLE III

CHARACTER TABLE OF D_{2d} POINT SYMMETRY GROUP (79)

D_{2d}	E	$2S_4$	$C_2^{(z)}$	$2C_2'$	$2\sigma_d$	
A_1	1	1	1	1	1	z^2
A_2	1	1	1	-1	-1	L_z
B_1	1	-1	1	1	-1	x^2-y^2
B_2	1	-1	1	-1	1	xy
E	2	0	-2	0	0	L_x, L_y ; xz, yz ; $q_{3b}\ q_{3c}$
$A_2 \times B_1$	1	-1	1	-1	-1	$= B_2$
$A_2 \times B_2$	1	-1	1	1	-1	$= B_1$
$A_2 \times E$	2	0	-2	0	0	$= E$
$B_1 \times B_2$	1	1	1	-1	-1	$= A_2$
$B_1 \times E$	2	0	2	0	0	$= E$
$B_2 \times E$	2	0	2	0	0	$= E$
$E \times E$	4	0	4	0	0	$= A_1 + A_2 + B_1 + B_2$

4.7 Hamiltonian

The tetravalent niobium ion Nb^{4+} can be thought of as a hydrogen-like ion, consisting of the krypton core of 36 electrons. We shall assume that the core electrons forms a spherical shell about the Nb nucleus. The Hamiltonian applicable to the free Nb ion is given by

$$\mathcal{H}_0 = -\frac{\hbar^2}{2m}\nabla^2 + V_0$$

where V_0 is a function of radius only.

Next we note that since the Nb ion is in the tungsten site, there are four oxygens near by. Then we have

$$\mathcal{H} = -\frac{\hbar^2}{2m}\nabla^2 + V_0 + V_1 + V_2 + V_3 + V_4$$

where the v_i's are the potential due to the four oxygens. If Nb is at the center of the bisphenoid, the potential will have the symmetry of D_{2d}. Then we have

$$V_1 + V_2 + V_3 + V_4 = V(D_{2d})$$

If we consider the effect of nuclear displacements with Nb off center, then we have

$$V_1 + V_2 + V_3 + V_4 = V(D_{2d}) + \text{linear terms of nuclear displacement} + \text{quadratic terms of nuclear displacement}$$

and so forth.

As indicated earlier, our model concerns only the q_{3b} and q_{3c} displacements. If we neglect terms higher than quadratic, we have

$$V_1 + V_2 + V_3 + V_4 = V(D_{2d}) + V'(\text{linear terms in } q_{3b}, q_{3c}) + V''(\text{quadratic terms in } q_{3b}, q_{3c})$$

If we classify the potential terms according to their symmetry properties, we have

$$V'(\text{linear terms in } q_{3b}, q_{3c}) \longrightarrow V'(E)$$

$$V''(\text{quadratic terms in } q_{3b}, q_{3c}) \longrightarrow V''(A_1) + V''(B_1) + V''(B_2)$$

The final Hamiltonian we shall use is therefore

$$H = -\frac{\hbar}{2m_1}\nabla^2 + V_0 + V(D_{2d}) + V'(E) + V''(A_1) + V''(B_1) + V''(B_2)$$

where we assume

$$V_0 > V(D_{2d}) > V'(E) + V''(A_1) + V''(B_1) + V''(B_2)$$

4.8 Energy Level Diagram

We shall in this section give the argument which lead to the energy level diagram as shown in Figure 26. From simple group theoretical consideration we know that the five $5d$ orbitals split into a triplet T_2 and a doublet E in a T_d field, but group theory does not tell which level is lower. If we consider the point charge model, we shall expect that the doublet E is lower and this is assumed to be valid in our case. If in addition to this T_d field there is also a D_{2d} field then the doublet E will further split into two singlets

A_1 and B_1 . The triplet T will further split into a singlet B_2 and a doublet E .

Since from the crystal structure of $CaWO_4$ it is known that the WO_4^{--} is very close to a regular tetrahedron, we can expect that the splitting due to D_{2d} field is very small compared to the splitting due to T_d field. Since the ESR spectrum can be observed at relatively high temperature (195°K) it indicates that the spin-lattice relaxation time is not too short. This is taken as evidence for the ground state being far away from the doublet E . Hence we can have either B_1 or A_1 as the ground state.

Using a point charge model of S_4 symmetry, Clyde Morrison[77] has obtained A_1 as the ground level. In this calculation Slater's radial wave functions were used and the oxygen atoms were assumed to be located as WO_4^{--}. The A_1 level was found to be the ground state for large variation of effective charge on the oxygen and for angular variation from WO_4^{--} (retaining S_4 symmetry) of several degrees. The A_1 state remained lowest for a large range of the spin-orbit constant. Since the tungstate is known to be covalent, we should not take the crystalline field result alone too seriously. However, the measured g-values do favor the assignment of A_1 being the ground level.

Experimentally, we have[78]

$$\Delta g_z = .053$$

$$\Delta g_y = .004$$

$$\Delta g_x = .012$$

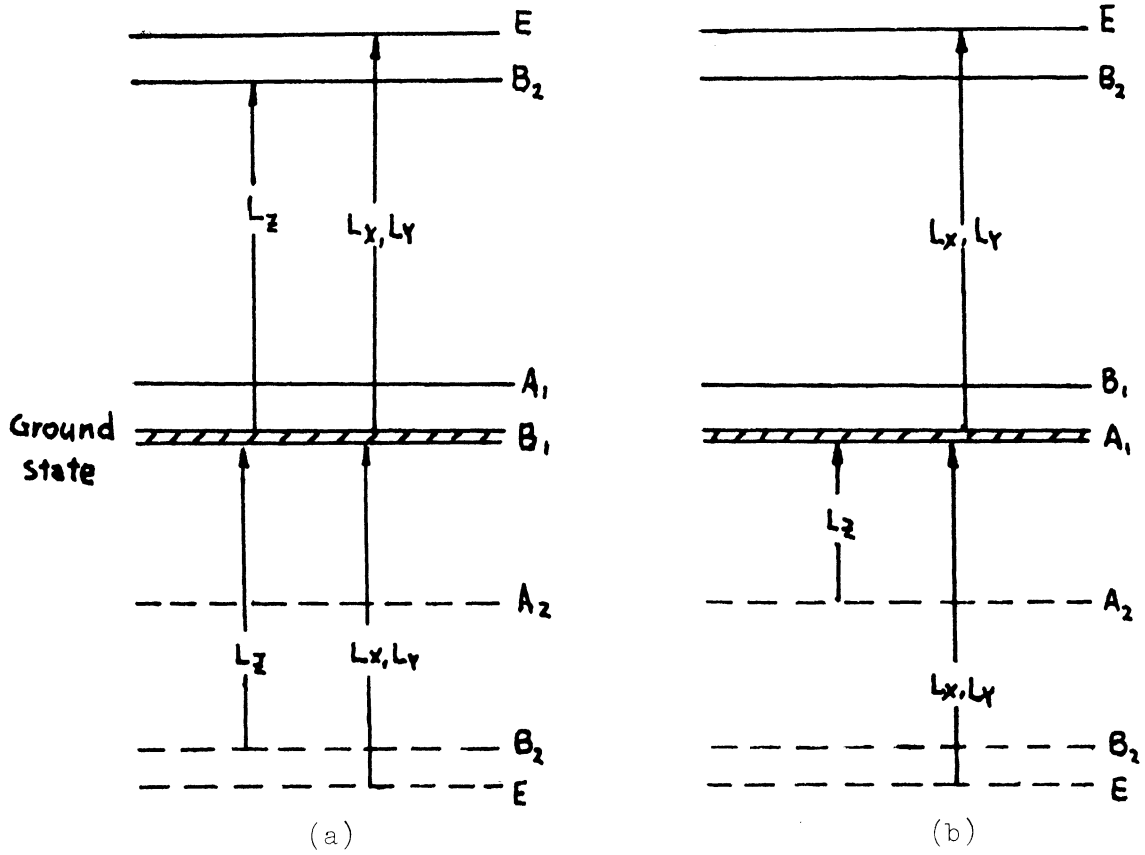

Figure 26. Energy Level Diagrams.

Notice that all Δg's are positive and particularly Δg_z is the largest. We shall try to get some information from the Δg-values. Since none of the Δg's vanish, the ground level should be connected to the remaining levels. From Table III, the symmetry of L_x, L_y and L_z are E, E and A_2 respectively. Using the direct products

$$B_1 \times E = E$$

$$B_1 \times A_2 = B_2$$

$$A_1 \times E = E$$

$$A_1 \times A_2 = A_2$$

we can sketch the energy level diagrams for B_1 and A_1 as the ground level with allowed crystal field and charge transfer transitions in Figure 26a and Figure 26b respectively.

For the case of B_1 being the ground level the crystal field transitions consist of B_1 level connected by L_z and E level connected by L_x, L_y. Since the observed Δg's is due to the difference between the charge transfer contribution and the crystal field contribution, unless there is a filled B_2 level very close to the ground level, we shall not have the observed large positive Δg_z.

For the case of A_1 being the ground level, there is no crystal field transition connected by L_z. The observed Δg_z is hence given by the contribution of charge transfer transition alone rather than the difference of charge transfer transition and the crystal field transition. The large observed Δg_z can be easily accounted for if there is a filled

A_2 level closer to the ground level than the filled E level. Thus we think that A_1 is more likely to be the ground level.

4.9 Perturbation Matrix

Using the energy level diagram just obrained and the perturbation Hamiltonian

$$\mathcal{H}' = V'(E) + V''(A_1) + V''(B_1) + V''(B_2)$$

the perturbation matrix is obtained, as follows.

	$A_1(z^2)$	$E^{(1)}(zx)$	$E^{(2)}(zy)$
$A_1(z^2)$	$V''(A_1)$	$V'(E)$	$V'(E)$
$E^{(1)}(zx)$	$V'(E)$	$D+V''(A_1)+V''(B_1)+V''(B_2)$	$V''(A_1)+V''(B_1)+V''(B_2)$
$E^{(2)}(zy)$	$V'(E)$	$V''(A_1)+V''(B_1)+V''(B_2)$	$D+V''(A_1)+V''(B_1)+V''(B_2)$

where D is the separation between E and A_1 levels. Simplification of the matrix elements have been made by using symmetry considerations. That is in order for the integral $\int \psi_f V \psi_i \, d\tau$ to be non zero the direct product of the representation of $\psi_f V \psi_i$ must be, or contain, the totally symmetric representation. This can only occur if the representation of the product of any two of the functions is, or contains, the same representation as the third function. In particular here we need only to consider the direct products $E \times B_2$, and $E \times E$,

From Table III we have $E \times B_2 = E$ and $E \times E = A_1 + A_2 + B_1 + B_2$. This gives the perturbation matrix mentioned above.

TABLE IV

CHARACTER TABLE OF D_2 GROUP

D_2	E	C_2^z	C_2^y	C_2^x	
A_1	1	1	1	1	x^2, y^2, z^2
B_1	1	1	-1	-1	L_z, xy
B_2	1	-1	1	-1	L_y, zx
B_3	1	-1	-1	1	L_x, zy

The perturbation matrix can be further simplified using the method of descending symmetry. Suppose we lower the symmetry from D_{2d} to D_2. The degeneracy of the E orbitals is now lifted. The correlation between them is

D_{2d}	D_2
A_1	A_1
A_2	B_1
B_1	A_1
B_2	B_1
E	B_2+B_3

The perturbation Hamiltonian is

$$\mathcal{H}' = V'(B_2) + V'(B_3) + V''(A_1) + V''(A_1) + V''(B_1)$$

With the help of Table IV, the following direct products of irreducible representations are obtained

$$A_1 \times A_1 = A_1$$

$$B_2 \times B_2 = A_1$$

$$B_3 \times B_3 = A_1$$

$$A_1 \times B_2 = B_2$$

$$A_1 \times B_3 = B_3$$

$$B_2 \times B_3 = B_1$$

From this we can have the following matrix

	$A_1(z^2)$	$B_2(zx)$	$B_3(zy)$
$A_1(z^2)$	$V''(A_1)$	$V''(E)$	$V'(E)$
$B_2(zx)$	$V'(E)$	$D + V''(A_1) + V''(B_1)$	$V''(B_2)$
$B_3(zy)$	$V'(E)$	$V''(B_2)$	$D + V''(A_1) + V''(B_1)$

The final form of the secular equation then takes the form

$$\begin{vmatrix} n(q_{3b}^2 + q_{3c}^2) - \Delta E & a q_{3b} & a q_{3c} \\ a q_{3b} & D + l_1(q_{3b}^2 + q_{3c}^2) + l_2(q_{3b}^2 - q_{3c}^2) - \Delta E & p q_{3b} q_{3c} \\ a q_{3c} & p q_{3b} q_{3c} & D + l_1(q_{3b}^2 + q_{3c}^2) + l_2(q_{3b}^2 + q_{3c}^2) - \Delta E \end{vmatrix} = 0$$

4.10 Energy Traps

As mentioned earlier, the WO_4^{--} is very close to a regular tetrahedron. We can expect $V''(B_1)$ to be much smaller than $V''(A_1)$. Thus we let $l_2 = 0$ and $l_1 = l$, and introduce the polar coordinates $q_{3b} = \rho \cos\varphi$ $q_{3c} = \rho \sin\varphi$ the secular equation then becomes

$$\begin{vmatrix} n\rho^2 - \Delta E & a q_{3b} & a q_{3c} \\ a q_{3b} & D + l\rho^2 - \Delta E & p q_{3b} q_{3c} \\ a q_{3c} & p q_{3b} q_{3c} & D + l\rho^2 - \Delta E \end{vmatrix} = 0$$

It gives

$$(n\rho^2 - \Delta E)(l\rho^2 - \Delta E + D) - a^2\rho^2(l\rho^2 - \Delta E + D)$$
$$- p(n\rho^2 - \Delta E)\frac{\rho^2}{8}(1 - \cos 4\varphi) + \frac{a^2 p}{4}\rho^2(1 - \cos 4\varphi) = 0$$

The appearance of the $\cos 4\varphi$ term in the energy expression makes it clear that there is a fourfold potential barrier. The extremization of the energy expression with respect to φ gives the condition

$$\sin 4\varphi = 0 \; ; \quad \therefore \varphi = m\pi/4 \quad , \quad m = 0, 1, 2, 3, 4, 5, 6, 7$$

If $m = 0, 2, 4, 6$ are the minimum points, each distorted configuration has only one two-fold symmetry axis and that will be along x- or y-axis in Figure 27. Therefore each of the four g-tensors has one of its principal axis parallel to the x- or y-axis. On the other hand if $m = 1, 3, 5, 7$ are the minimum points, each distorted configuration will have a reflection plane and that will be the diagonal

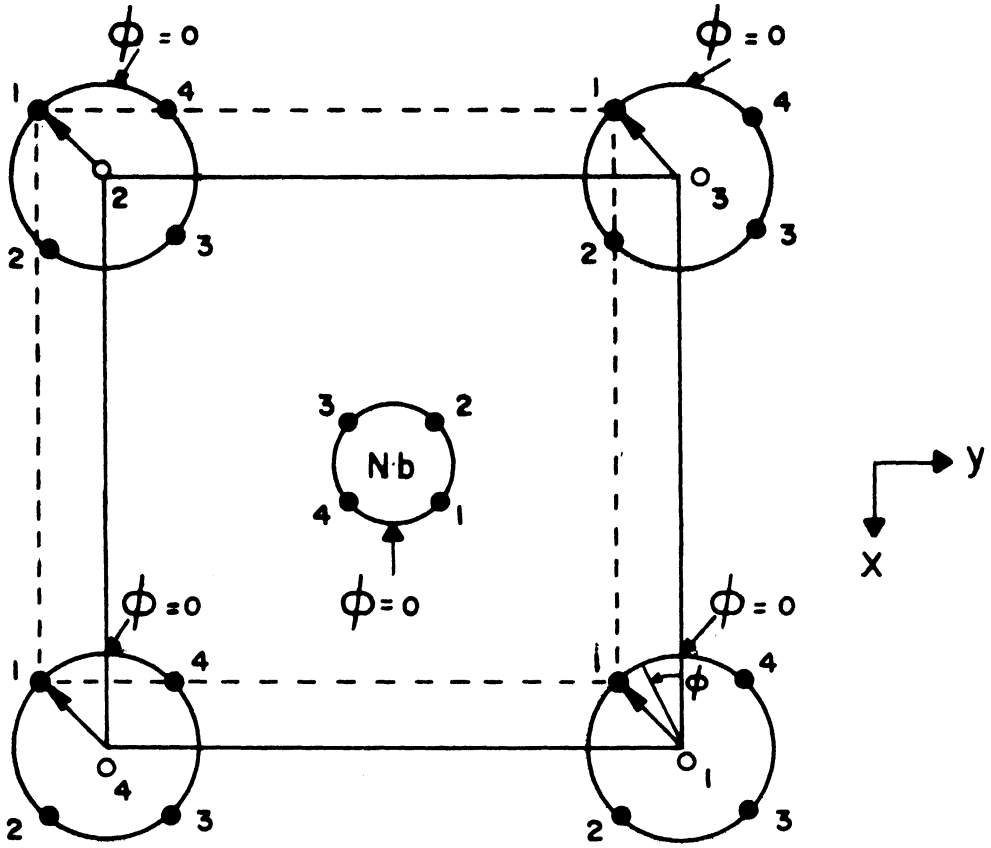

1. $\phi = \pi/4$
2. $\phi = 3\pi/4$
3. $\phi = 5\pi/4$
4. $\phi = 7\pi/4$

Figure 27. Nuclear Vibration of NbO_4^{--} with Projection on the (ab)-plane.

planes of the bisphenoid. Therefore each of the four g-tensors has one of its principal axis perpendicular to the diagonal planes.

Experimentally, from Figure 23 we know the four g-values become identical in the (ab) plane with 17° from the a-axis or only 4° from the x- or y-axis in Figure 27. If any principal axis of the four g-tensors is in the (ab) plane it will have to be $\sim\pi/4$ from the x- or y-axis rather than parallel to the axes. Hence the experimental results require that the minima of energy occur at

$$\varphi = m\pi/4, \quad m = 1, 3, 5, 7$$

and the saddle points at

$$\varphi = m\pi/4, \quad m = 0, 2, 4, 6$$

The situation can be summarized as follows: If the only active nuclear vibration is the doubly degenerate mode of q_{3b} and q_{3c}, the NbO_4 radical will execute motion in the (ab)-plane. The nuclear motion is shown in Figure 27. There are four energy traps at $\varphi = \pi/4, 3\pi/4, 5\pi/4$ and $7\pi/4$. The configuration of minimum energy corresponds to one of the four oxygen nuclei and the central niobium nucleus moving closer to each other and the remaining three oxygen nuclei moving farther from the central niobium nucleus. The only symmetry elements of this distorted bisphenoid is a reflection plane. These are the diagonal planes. The g-tensor will have one principal axis perpendicular to the reflection plane (in the (ab)-plane) and two principal axes in the reflection plane. One of the two is likely along the closest Nb-O direction.

At low temperature the radical is frozen in to one of the four potential traps. Since the g-tensors corresponding to each trap are different (principal values are the same but orientations of the principal axes are different) four sets of lines are observed. At higher temperature the radical can override the potential barriers and only one set of lines is observed at the average position of the four low temperature sets.

5. CONCLUSIONS

The results of the investigation of reactor fast neutron irradiated calcium tungstate single crystals leave little doubt that two kinds of paramagnetic tungsten centers associated with oxygen and calcium vacancies respectively are produced. The identification of the gamma-center as paramagnetic tungsten with a nearest oxygen displaced is based on the following evidence:

a. Hyperfine interaction due to tungsten isotope W^{183} ($I = 1/2$, 14.24% natural abundance) is observed. Each ESR line is flanked by two satellites with intensity ratio 1:12:1.

b. One principal axis of the g-tensor is along one of the tungsten-oxygen bond directions and the angular variation of the spectrum follows the model of paramagnetic tungsten with a nearest displaced oxygen.

c. Uniaxial stressed ESR result provides further support of this assignment.

d. The experimental g-values can be accounted for qualitatively by assuming an unpaired 5d electron on the tungsten subject to the electric crystalline field of three nearest oxygens of the predominantly C_{3v} symmetry and a smaller C_s symmetry.

e. The gamma-center is very stable at room temperature but can be completely annealed out by heating up to 600°C.

Almost the same arguments lead to the identification of the beta-center as paramagnetic tungsten with a nearest calcium displaced. Since the gamma-center is quite stable up to 60°C which is equal to

the irradiation temperature it is reasonable to assume that little annealing is experienced during irradiation. The measurement of defect concentration provides one of the few opportunities to compare with radiation damage theory. It is interesting to recall that in literature[50] except for a few cases, most of the experimentally measured defect concentration are five to ten times less than the theoretical values predicted by simple radiation damage theory. But in the few exceptional cases, experiments are carried out by the so-called direct methods such as the F-center measurement by Levy[39] and the slow neutron scattering method by Antal.[40] By direct methods it means that the measured quantity is more directly connected to the defect concentration. In spite of the possibly more complicated defect formation mechanism such as spikes, focussing and channeling and so forth, the simple radiation damage theory of Kinchin and Pease is found in good agreement with the gamma-center concentration obtained by ESR measurement.

The study of Co^{60} gamma-ray irradiated $CaWO_4$: Nb^{4+} single crystals leads to the following conclusions: Before irradiation, niobium in W-site forms the diamagnetic complex NbO_4^{--} . After irradiation, it acquires one electron and becomes paramagnetic NbO_4^{3-} . At 195°K, the spectrum can be described by the spin-hamiltonian

$$\mathcal{H} = \beta\left[g_{\parallel} S_z H_z + g_{\perp}(S_x H_x + S_y H_y)\right] + A I_z S_z + B(I_x S_x + I_y S_y)$$

with $S = 1/2$, and $I = 9/2$. The measured coupling constants are

$$g_{\parallel} = 2.023 , \qquad g_{\perp} = 2.026$$

$$A = 29 \text{ gauss} , \qquad B = 29.2 \text{ gauss}$$

where the axial symmetry axis is along the crystal c-axis.

The temperature dependence of the spectrum can be explained by the effect of vibronic interactions. At low temperatures the NbO_4^{3-} radical is frozen into one of the four potential traps, and it assumes the shape of a distorted bisphenoid with one of the Nb-O bond compressed. At temperatures so high that the NbO_4^{3-} radical has sufficient energy to override the barriers, the complex will exhibit a sort of pseudo rotation and all of the nuclei perform a coupled rotation. This accounts for the high temperature spectrum.

Since the only spectrum observed is due to substitutional niobium in tungstate site, it is the direct evidence that all of the niobium atoms are in the W-site which has only been inferred previously from chemical evidence.

APPENDIX

g-VALUES OF THE GAMMA-CENTER

The experimental results obtained about the g-values of the gamma-center are as follows:

$$g_z = 1.914 \qquad \Delta g_z = -0.088$$
$$g_x = 1.675 \qquad \Delta g_x = -0.327$$
$$g_y = 1.646 \qquad \Delta g_y = -0.356$$

Notice that $|\Delta g_z|$ is small compared to $|\Delta g_x|$ and $|\Delta g_y|$. Furthermore Δg_x is nearly equal to Δg_y. This suggests that as a first approximation the three nearest oxygens to the tungsten form a equilateral triangle (Figure 28). But in this case Δg_z will be equal to zero. If the symmetry is lowered to C_s, (Figure 28, that is the actual symmetry of the gamma-center from the crystal structure) we can account for the result $g_z > g_x \sim g_y$. All these can be shown as follows:

To account for the observed results we shall then assume that a paramagnetic $W^{5+}(5d')$ ion is subject to the strong electrostatic field of the three nearest oxygens. As indicated already, these three oxygens form the base of a triangular prism, with the tungsten located at the apex. We shall first assume the oxygens form an equilateral triangle. The character table for the C_{3v} group is[79]

	E	$2C_3$	3
A_1	1	1	1
A_2	1	1	-1
E	2	-1	0

Defect Model

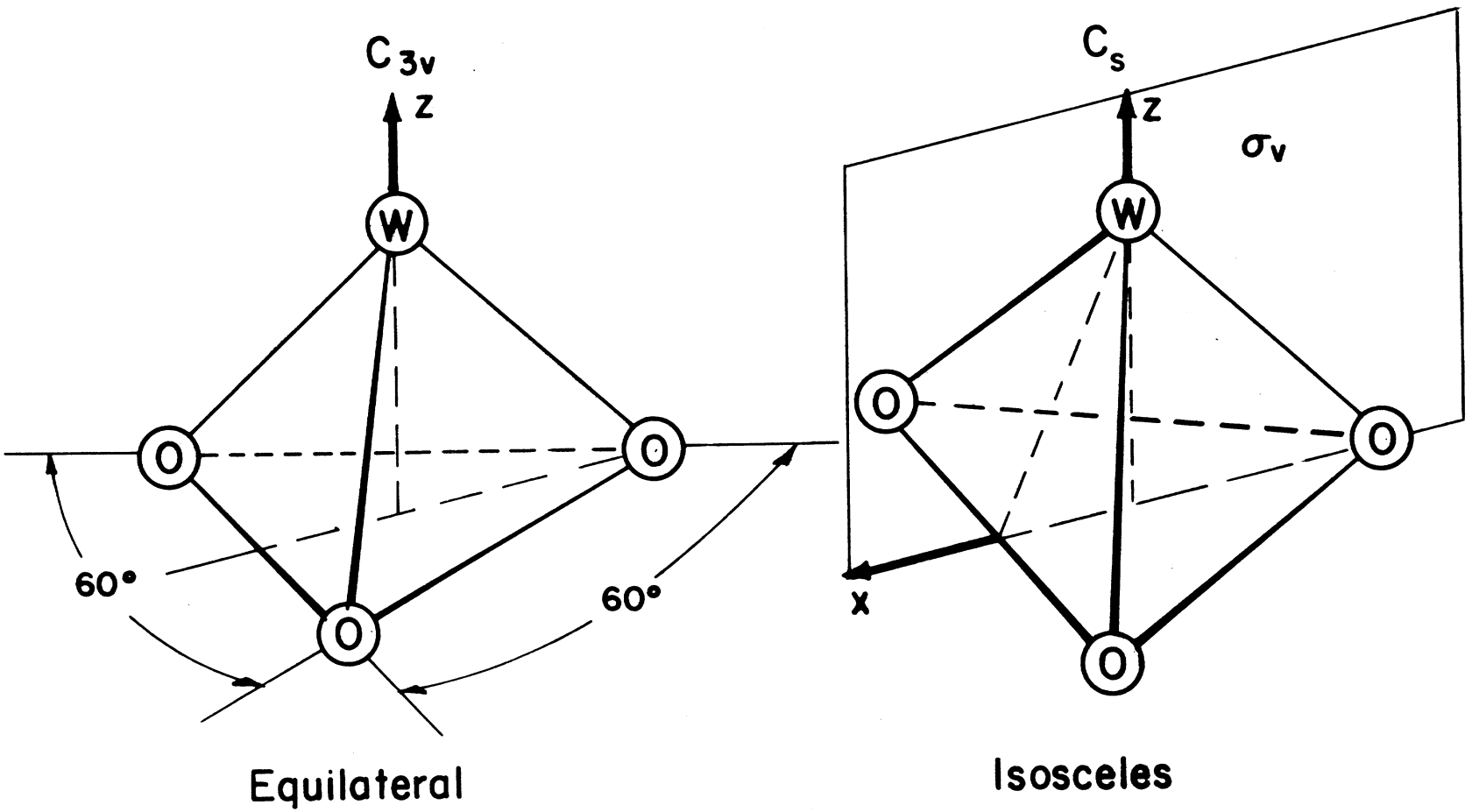

Figure 28. Defect Models of the γ-center.

We wish to use this table to deduce some general information about the nature of the electron energy levels as affected by the three ligand oxygens.

The mathematical significance of the statement that the extra unpaired electron is on the tungsten is that the angular part of the electron involves the spherical harmonics $\ell = 2$. The electron energy level, in the absence of the ligand oxygens, will be $2\ell + 1$ fold degenerate. Energy levels can be split by the Stark effect. In the present problem, the stark effect is produced by the electric field arising from the ligand oxygens.

To determine the manner in which the energy levels will split, we need first to determine the so-called characters of the reducible representation. These are determined from the matrices generated by the operations of the C_{3v} group upon the column vector of Y_{2m} spherical harmonics. Thus

$$R \begin{pmatrix} Y_{2\bar{2}} \\ Y_{2\bar{1}} \\ Y_{20} \\ Y_{21} \\ Y_{22} \end{pmatrix} = \begin{pmatrix} & 5 \times 5 & \end{pmatrix} \begin{pmatrix} Y_{2\bar{2}} \\ Y_{2\bar{1}} \\ Y_{20} \\ Y_{21} \\ Y_{22} \end{pmatrix}$$

Since there are six elements in the group, there are six, 5 by 5 matrices. The matrices generated in this manner will be denoted by $\Gamma(R)$. The matrix generated by the identity element E has 1 along the diagonal but zero everywhere else. Thus

$$\Gamma(E) = \begin{pmatrix} 1 & 0 & 0 & 0 & 0 \\ 0 & 1 & 0 & 0 & 0 \\ 0 & 0 & 1 & 0 & 0 \\ 0 & 0 & 0 & 1 & 0 \\ 0 & 0 & 0 & 0 & 1 \end{pmatrix}$$

so that its character, or the diagonal sum is five, i.e.

$$\chi(E) = 5$$

Consider next the effect of 120° rotations about the z-axis. For this we note that the spherical harmonics can be written in the form

$$Y_{lm}(\theta,\varphi) = P_{lm}(\cos\theta)\frac{1}{\sqrt{2\pi}}e^{im\varphi}$$

The effect of any rotation Φ about the z-axis, is

$$\varphi \longrightarrow \varphi + \Phi$$

As a consequence, all spherical harmonics will be multiplied by the factor

$$e^{im\Phi}$$

Hence the matrix generated by this rotation is given by

$$\begin{pmatrix} e^{-il\Phi} & 0 & 0 & 0 \\ 0 & e^{-i(l-1)\Phi} & 0 & 0 \\ & & \ddots & \\ 0 & 0 & e^{i(l-1)\Phi} & 0 \\ 0 & 0 & 0 & e^{il\Phi} \end{pmatrix}$$

The trace or the diagonal sum is easily shown to be

$$\chi(\Phi) = \frac{\sin(\ell+\frac{1}{2})\Phi}{\sin \Phi/2}$$

Therefore for $\ell = 2, \Phi = 2\pi/3$, we find that

$$\chi(C_3) = -1$$

To determine the character for the reflections σ_v, we note that a reflection is equivalent to rotation by 180° about an axis normal to the reflection plane followed by an inversion. Putting $\Phi = \pi$ in the earlier expression and noting that the degree of spherical harmonic is even we find that

$$\chi(\sigma_v) = +1$$

We have thus found that

	E	$2C_3$	$3\sigma_v$
χ_d	5	-1	1

Comparing these with those of the character table we find that

$$\chi_d = \chi_{A_1} + 2\chi_E$$

The physical interpretation of this mathematical results is that the five-fold degenerate d-level will split into three levels, one of which has the symmetry A_1 and the remaining two have the symmetry E. The A_1 level is non-degenerate. The energy level diagram and wave functions are shown in Figure 29.

C_{3v} Symmetry

CHARACTER TABLE

	E	$2C_3$	$2\sigma_v$
A_1	1	1	1
A_2	1	1	-1
E	2	-1	0
x(d)	5	-1	1

$$x(d) = x(A_1) + 2x(E)$$

$E^{(2)}$ ——— $\sqrt{3}\,zy$, $\sqrt{3}\,zx$

$E^{(1)}$ ——— $\frac{\sqrt{3}}{2}(x^2-y^2)$, $\sqrt{3}\,xy$

A_1 ——— $\frac{3z^2-r^2}{2}$

$\Delta_z g = 0, \quad \Delta g_x, \Delta g_y < 0$

Figure 29. Character Table and Energy Level Diagram for the Defect of C_{3v} Symmetry.

The g-values or to be more precise, the Δg's , are defined by

$$\Delta g_j = g_j - g_e$$

where g_e is the spectroscopic splitting factor of the free electron having the numerical value 2.0023. Δg's are obtained from the expression[80,76]

$$\Delta g_j = -\frac{\lambda}{E_f - E_i} \left| \langle \psi_f | L_j | \psi_i \rangle \right|^2$$

For Δg_z , we have

$$\Delta g_z = -\frac{\lambda}{E_f} \left| \langle \psi_f | L_z | \psi_i(A_1) \rangle \right|^2$$

Since L_z transforms like A_1 and the product $L_z \psi_i(A_1)$ transforms like $A_1 \times A_1 = A_1$, the symmetry of the final state must be A_1 for the matrix element not to vanish. Since there is no A_1 level aside from the ground level in the diagram that has been presented, we concluded that $\Delta g_z = 0$, for C_{3v} symmetry.

In order to account for the observed result $\Delta g_z \neq 0$ and $g_z > g_x \sim g_y$, we need to take distortion from C_{3v} symmetry into account. From the crystal structure, three oxygens actually form an isosceles triangle, so that we need to introduce a perturbation of symmetry C_s . The character table for this group is[79]

	E	σ_v
A'	1	1
A''	1	-1

The effect of this perturbation can be depicted graphically as shown in

Figure 30. The angular momentum operators L_z, L_x and L_y transform like A'', A'' and A', so that the matrix elements relevant in calculating Δg's are

$$\Delta g_z = -\frac{\lambda |\langle A''(2)|L_z|A'\rangle|^2}{E(A''(2))} - \frac{\lambda |\langle A''(3)|L_z|A'\rangle|^2}{E(A''(3))}$$

$$\Delta g_x = -\frac{\lambda |\langle A''(2)|L_x|A'\rangle|^2}{E(A''(2))} - \frac{\lambda |\langle A''(3)|L_x|A'\rangle|^2}{E(A''(3))}$$

and

$$\Delta g_y = -\frac{\lambda |\langle A'(2)|L_y|A'\rangle|^2}{E(A'(2))} - \frac{\lambda |\langle A'(3)|L_y|A'\rangle|^2}{E(A'(3))}$$

The following table is useful in evaluating the matrix elements,

	d_{z^2}	$d_{x^2-y^2}$	d_{zx}
L_z	0	$2i\,d_{xy}$	$i\,d_{yz}$
L_x	$-i\sqrt{3}\,d_{yz}$	$-i\,d_{yz}$	$-i\,d_{xy}$
L_y	$i\sqrt{3}\,d_{zx}$	$-i\,d_{zx}$	$-i\sqrt{3}\,d_{z^2} + i\,d_{x^2-y^2}$

If the ground level is denoted by

$$N_1 \frac{3z^2-r^2}{2} + N_2 \frac{\sqrt{3}}{2}(x^2-y^2) + N_3\, zx$$

and the coefficients $N_1 > N_2 > N_3$, then

$$\Delta g_z = -\frac{4\lambda N_2^2}{E(A''(2))}$$

$$\Delta g_x = -\frac{\lambda(\sqrt{3}N_1 + N_2)^2}{E(A''(3))}$$

$$\Delta g_y = -\frac{\lambda(\sqrt{3}N_1 - N_2)^2}{E(A'(3))}$$

This accounts for the experimental result $\Delta g_z \neq 0$ and $g_z > g_x \sim g_y$ if $E(A''(3)) \sim E(A'(3))$.

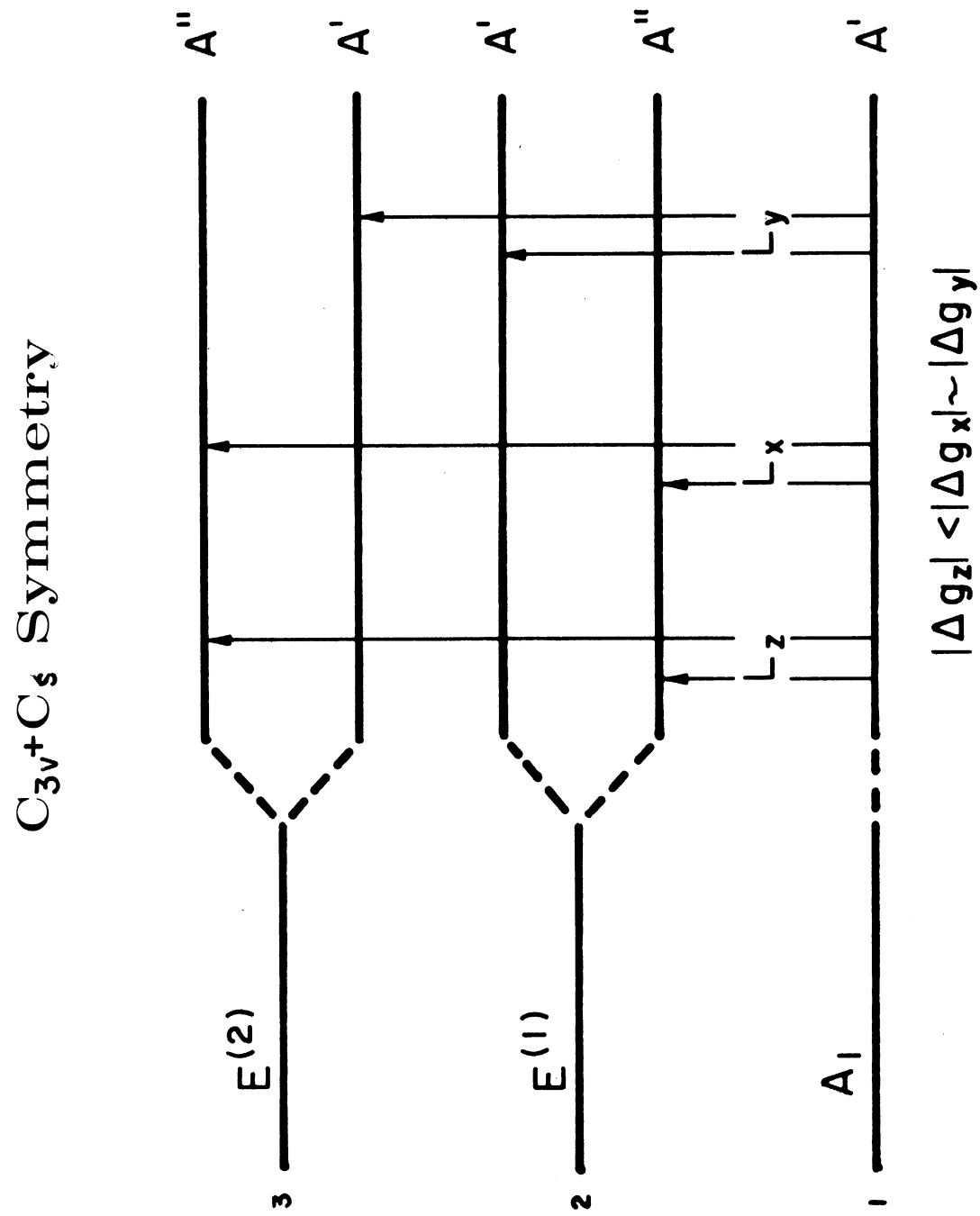

Figure 30. Energy Level Diagram for the Defect of C_s Symmetry.

REFERENCES

1. L. F. Johnson. "Optical Maser Characteristics of Rare-Earth Ions in Crystals." J. A. Phys. 34, 847 (1963).

2. L. F. Johnson and K. A. Thomas. "Master Oscillations at 0.9 and 1.35 Microns in $CaWO_4$: Nd^{3+}." Phys. Rev. 131, 2038 (1963).

3. P. Golich, H. Karras, G. Kotitz and Lehmann. "Spectroscopic Properties of Activated Laser Crystals." Physica Status Solidi, 5, 437 (1964); 6, 277 (1964); 8, 385 (1965).

4. L. F. Johnson. "Characteristics of the $CaWO_4$: Nd^{3+} Optical Masers." Quantum Electronics, Paris, Vol. 2,1021 (1963).

5. C. F. Hempsted and K. D. Bowers. "Paramagnetic Resonance of Impurities in $CaWO_4$.I. Two S-State Ions." Phys. Rev. 118, 131 (1960).

6. P. A. Forrester and C. F. Hempstead. "Paramagnetic Resonance of Tb Ions in $CaWO_4$ and CaF_2." Phys. Rev. 126, 923 (1962).

7. R. W. Kedzie and M. Kestigian. "PMR Determination of Transition Metal Ions and Multiplicity of Rare-Earth Ion Sites in $CaWO_4$." Appl. Phys. Let. 3, 86, (1963).

8. R. W. Kedzie and M. Kestigian. "PMR of Nd^{3+} in $CaWO_4$." Appl. Phys. Let. 4, 124 (1964).

9. C. G. B. Garrett and F. R. Merritt. "PMR Spectra of Nd^{3+} in Compensated and Uncompensated $CaWO_4$." Appl. Phys. Letters, 4, 31 (1964).

10. T. U. Ranon. "Electron Spin Resonance of $CaWO_4$: Nd^{3+}." Phys. Let. 8, 154 (February, 1964).

11. J. Kirton. "PMR of Ho^{3+} Ions in $CaWO_4$." Phys. Rev. 139, A1930 (1965).

12. I. Z. Potvorova and La. Ya. Shekun. "EPR Study of Tetragonal Sm Centers in $CaWO_4$." Sov. Phys. Solid-State 7, 2596, (1966).

13. J. Bronstein and V. Volterra. "EPR of Eu^{2+} in $CaWO_4$." Phys. Rev. 137, A1201 (1965).

14. R. H. Gillette. "Calcium and Cadmium Tungstate As Scintillation Counter Crystals for Gamma-Ray Detection." Rev. Sci. Inst. 21, 294, (April, 1950).

15. M. Sayer and W. R. Hardy. "Scintillation Decay in Calcium Tungstate." Canadian J. of Phys. 43, 1925 (1965).

16. K. Nassau and A. M. Broyer. "Calcium Tungstate: Czochralski, Growth, Perfection and Substitutions." J. Appl. Phys. 33, 3064 (1962).

17. K. Nassau and G. M. Loiacono. "Calcium-Tungstate, Trivalent Rare-Earth Substitution." J. Phys. Chem. Solids, 24, 1503 (1963).

18. K. Nassau. "Calcium Tungstate-IV, Theory of Coupled Substitution." J. Phys. Chem. Solids, 24, 1511 (1963).

19. A. Zalkin and D. H. Templeton. "X-Ray Diffraction Refinement of the $CaWO_4$ Structure." J. Chem. Phys. 40, 501 (1964).

20. M. I. Kay, B. C. Grazer and I. Almodovar. "Neutron Diffraction Refinement of $CaWO_4$." J. Chem. Phys. 40, 504 (1964).

21. E. Zaviosky. "Spin Resonance in the Decimeter Range." J. Phys. USSR, 10, 197 (1946).

22. R. L. Cummerow and D. Halliday. "Paramagnetic Loses in Two Manganous Salts." Phys. Rev. 70, 433 (1946).

23. Helmut Beinert and Graham Palmer. "Contribution of EPR Spectroscopy to Our Knowledge of Oxidative Enzymes." Advances in Enzymology, Vol. 27, Interscience (1965).

24. Wallace Snipes. "Electron Spin Resonance and the Effects of Radiation on Biological Systems." National Academy of Sciences (1966).

25. C. Kikuchi, S. Chen and S. Yip. "Application of ESR to the Study of Radiation Effects." Neutron Phys. Conf. Mackinac. (61).

26. G. E. Pake. Paramagnetic Resonance. Frontiers in Physics Series, Benjamin (1962).

27. M. Bersohn. An Introduction to Electron Paramagnetic Resonance. Benjamin, (1966).

28. J. D. E. Ingram. Spectroscopy at Radio and Microwave Frequencies. Academic Press (1955).

_____. Free Radicals as Studied by Electron Spin Resonance. Academic Press (1958).

29. C. P. Slichter. Principle of Magnetic Resonance. Harper and Row, (1963).

30. B. Bleaney and K. W. H. Stevens. "Paramagnetic Resonance." Repts. Prog. Phys. 16, 108 (1953).

31. K. D. Bowers and J. Owen. "Paramagnetic Resonance." Repts. Prog. Phys. 18, 304 (1955).

32. H. S. Jarrett. "Electron Spin Resonance Spectroscopy in Molecular Solids." Solid State Phys. Vol. 14 (1963).

33. D. K. Wilson. "ESR Experiments on Shallow Donors in Germanium." Phys. Rev. 134, A256 (1964).

34. E. R. Feher. "Effects of Uniaxial Stress on Paramagnetic Spectra of Mn^{++} and Fe^{3+} in MgO." Phys. Rev. 136, A145 (1964).

35. G. Feher, J. Hensel and E. Gere. "Paramagnetic Resonance Absorption from Acceptors in Silicon." Phys. Rev. Lett. 5, 309 (1960).

36. G. D. Watkins and J. W. Corbett. "Defects in Irradiated Silicon, ESR of the Si-A Center." Phys. Rev. 121, 1001 (1961).

37. W. Kanzig. "Paraelasticity, A Mechanical Analog of Paramagnetism." Phys. Chem. Solids, 23, 479 (1962).

38. G. D. Watkins and J. W. Corbett. "Defects in Irradiated Silicon, ESR and ENDOR of the Si-E Center." Phys. Rev. 134, A1359, (1964).

39. P. W. Levy. "Direct Measurement of the Vacancies Produced in NaCl by Fast Reactor Neutrons." Phys. Rev. 129, 1076 (1958).

40. J. Antal, et al. "Long Wavelength Neutron Transmission as an Absolute Method for Determining the Concentration of Lattice Defects in Crystals." Phys. Rev. 99, 1081 (1955).

41. G. J. Dienes and G. H. Vineyard. "Radiation Effects in Solids." Interscience, (1957).

42. D. S. Billington and J. H. Crawford, Jr. "Radiation Damage in Solids." Princeton University Press (1961).

43. R. Strumane, J. Nihoul, R. Gevers and S. Amelinckx. "The Interaction of Radiation with Solids." North-Holland (1964).

44. F. Seitz and J. S. Kohler. "Displacement of Atoms during Irradiation." Solid State Phys. Vol. 2, (1956).

45. J. W. Corbett. "Electron Radiation Damage in Semiconductors and Metals." Solid State Phys. Supp. 7 (1966).

46. Seventh International Conference on the Physics of Semiconductors. "Radiation Damage in Semiconductors." Academic (1964).

47. D. S. Billington. Radiation Damage in Solids. Academic Press (1962).

48. G. Leibfried. Bestrahlungseffekte in Festkorpern. Teubner Verlagsgesellschaft (1965).

49. L. T. Chadderton. "Radiation Damage in Crystals." John Wiley and Sons, Inc. (1965).

50. Symposium on the Chemical and Physical Effects of High Energy Radiation on Inorganic Substances. ASTM Special Technical Publication, No. 359 (1963).

51. Chr. Lehmann. "Zur Bildung von Defekt-Kaskaden in Kristallen beim Beschuss mit Energiereichen Teilchen." Nukleonik, Band 3, Heft 1 (1961).

52. A. E. Fein. "Influence of a Variable Ejection Probability on the Displacement of Atoms." Phys. Rev. 109, 1076 (1958).

53. G. Leibfried. "Statistische Schwankungen der von einem Primateilchen Erzeugten Frenkel-Defekte." Nukleonik, Band 1, Heft 2 (1958).

54. E. H. Baroody. "Influence of Mass Ratio on Displacement Cascades in Diatomic Solids." Phys. Rev. 112, 1571 (1958).

55. L. Harris, Jr.; G. Sherwood and J. S. King. "Fast Neutron Spectra in Water and in Graphite." Nucl. Sci. and Eng. 26, 571 (1966).

56. United States Atomic Energy Commission. "Research Reactors." McGraw-Hill Co., New York (1955).

57. Part of these results has been published in IEEE Transaction Nuclear Science, NS-13, 41 (1966).

58. H. Zeldes and R. Livingston. "Paramagnetic Resonance Study of Irradiated Single Crystals of Calcium Tungstate." J. Chem. Phys. 34, 247 (1961).

59. Nuclear Moments by Norman Ramsey, John Wiley, New York (1953).

60. H. Azarbayejani. "ESR of W^{54} in $CaWO_4$: Y." Bull. Am. Phys. Soc. Vol., 10, No. 8, 1138 (1965).

61. D. M. S. Bagguley and J. H. Griffiths. "Paramagnetic Resonance in Copper Sulphate." Proc. Roy. Soc. A201, 36 (1950).

62. L. S. Singer. "Synthetic Ruby as a Secondary Standard for the Measurement of Intensities in EPR." J.A.P. 30, 1463 (1959).

63. R. H. Hoskins and R. C. Pastor. "Charred Dextrose as a Paramagnetic Resonance Standard." J.A.P. 31, 1506 (1960).

64. R. H. Silsbee. "F-Band Oscillator Strength Determination in NaCl and KCl." Phys. Rev. 103, 1675, (1956).

65. V. R. Burgess. "Analogue Method for Computing the Number of Spins Contributing to a Magnetic Resonance Absorption." J. Sci. Inst. 38, 98 (1961).

66. L. S. Singer and G. Wagoner. "ESR in Polycrystalline Graphite." J.C.P. 37, 1812 (1962).

67. L. S. Singer, W. Spry and W. Smith. "EPR in Charred Sucrose." Proc. Con. Carbon, 3rd. pp. 121, (1959).

68. R. Schumacher and C. Slichter. "Electron Spin Paramagnetism of Lithium and Sodium." Phys. Rev. 101, 58 (1959).

69. L. S. Singer and J. Kommandeur.""ESR in Complex of Aromatic Hydrocarbons with Iodine." J.C.P. 34, 133, (1961).

70. R. T. Weidner and C. A. Whitmer. "The Shape of Exchange Narrowed Paramagnetic Resonance Lines." Phys. Rev. 91, 1279 (1953).

71. Part of this study has been published in J. Chem. Phys. 46, 386 (1967).

72. N. Mahootian. An ESR Study of Vanadium in Calcium Tungstate Crystals Ph.D. Thesis Dept. of Nuclear Engineering, University of Michigan (1966).

73. Vinokurov, et al. "Paramagnetic Resonance of Nb^{4+} Ion in Zircon Single Crystals." Soviet Phys. Solid-State 5, 1487 (1964).

74. P. Chester. "Cross-Doping Agents for Rutile Masers." J. Appl. Phys. 32, 866 (1961).

75. P. Rasmussen. "ESR of Pentachloromethoxoniobate." Inorganic Chem. 4, 343 (1965).

76. Sophocles Karavelas. Molecular Orbital Theory of V in the Rutile Structure Crystals SnO_2, TiO_2 and GeO_2. Ph.D. Thesis, Dept. of Nuclear Eng. University of Michigan (1964).

77. Private communication.

78. Unpublished results measured by Der-ling Tseng.

79. V. Heine. Group Theory in Quantum Mechanics. Pergamon Press New York (1960).

80. M. H. L. Pryce. "A Modified Perturbation Procedure for a Problem in Paramagnetism." Proc. Phys. Soc. (London) A63, 25 (1950).

81. A. Liehr. "Topological Aspects of the Conformational Stability Problem." J. Phys. Chem. 67, 389 (1963).

UNIVERSITY OF MICHIGAN
3 9015 02829 5155